Supplement of Geosci. Model Dev., 14, 7345–7376, 2021
https://doi.org/10.5194/gmd-14-7345-2021-supplement

Geoscientific Model Development
Open Access
EGU

Supplement of

STEMMUS-UEB v1.0.0: integrated modeling of snowpack and soil water and energy transfer with three complexity levels of soil physical processes

Lianyu Yu et al.

Correspondence to: Yijian Zeng (y.zeng@utwente.nl) and Zhongbo Su (z.su@utwente.nl)

Contents

S1. Overview of Coupled Soil-Snow Modelling Framework: STEMMUS-UEB

STEMMUS-UEB simulates water and energy fluxes between the land surface and the atmosphere accounting for the water and energy exchange across various interfaces, i.e., root-soil, soil-atmosphere, vegetation-atmosphere, soil-snow, snow-atmosphere. The model is specialized in solving the vadose zone physical process by interpreting it with multi-level complexity. It describes the vadose zone processes including soil water, vapor, dry air, and energy transfer, root water uptake, and freeze-thaw (STEMMUS-FT component). Moreover, snowpack processes, snow accumulation, melting, ablation, are implemented via the UEB module. Multiple processes are interactively represented in the model, reproducing the underlying physics of the soil-snow-atmosphere system. The interactive dynamics of water and energy across different interfaces are numerically solved by STEMMUS-UEB with the local meteorological forcing, boundary conditions, and soil/snow/vegetation properties. The operational time scale is flexible from minutes to daily, and further long term simulations. Currently, local scale simulation is resolved while it has the potential to conduct large scale simulations taking advantage of the remote sensing and reanalysis data. The conceptual coupling soil-snow-atmosphere framework is illustrated in Figure S1.1. An outline of the simulated physical processes and model structure is presented in Figure S1.2. The general development and application of soil and snowpack submodules are briefly introduced in Section S1.1 and S1.2.

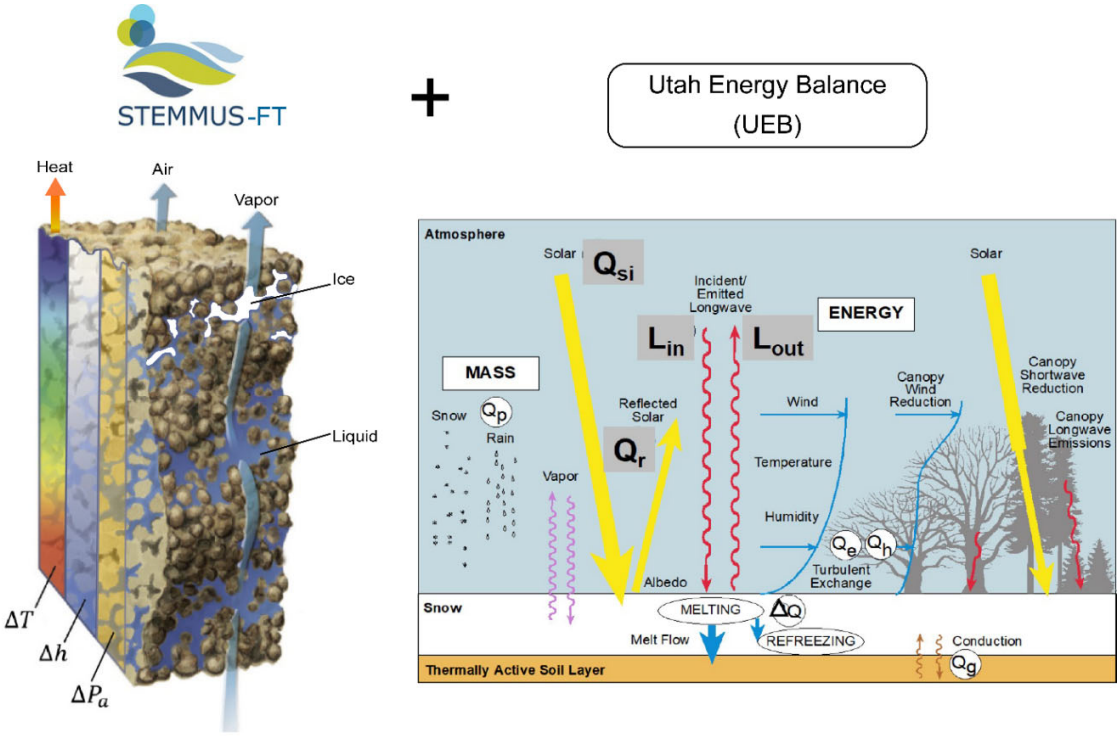

Figure S1.1. The conceptual figure of coupled soil-snow-atmosphere modeling framework. The UEB module is adapted from Tarboton and Luce (1996). $\Delta T, \Delta h, \Delta P_a$ are the vertical gradient of soil temperature, matric potential, and air pressure, respectively.

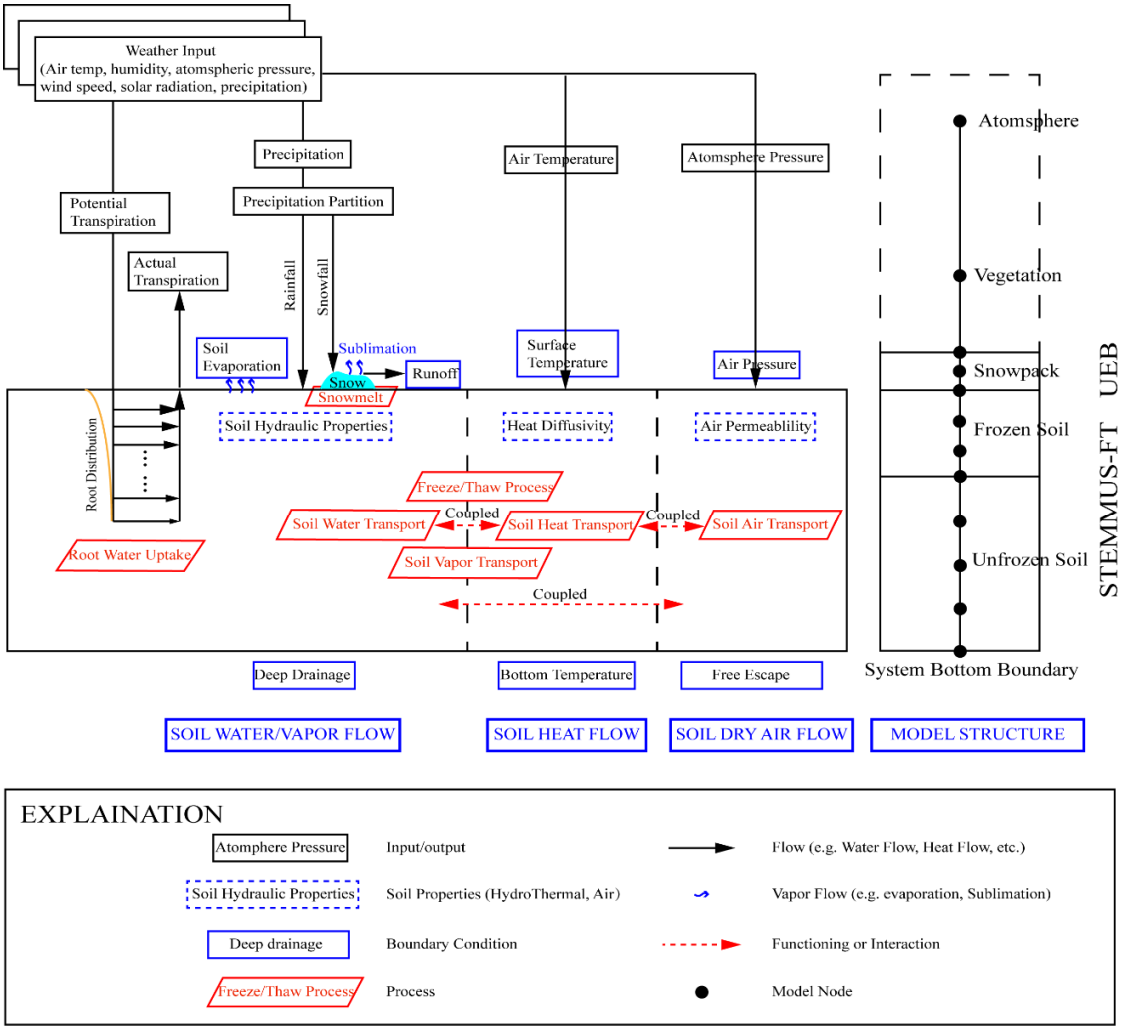

Figure S1.2. The schematic figure illustrating the input/output, boundary conditions, relevant physical processes, and model structure of STEMMUS-UEB.

S1.1 Soil module

The detailed physically based two-phase flow soil model (**S**imultaneous **T**ransfer of **E**nergy, **M**omentum and **M**ass in **U**nsaturated **S**oil, STEMMUS) was first developed to investigate the underlying physics of soil water, vapor, and dry air transfer mechanisms and their interaction with the atmosphere (Zeng et al., 2011b, a; Zeng and Su, 2013). It is realized by simultaneously solving the balance equations of soil mass, energy, and dry air in a fully coupled way. The mediation effect of vegetation on such interaction was latterly incorporated via the root water uptake sub-module (Yu et al., 2016) and furthermore by coupling with the detailed soil and vegetation biogeochemical processes (Wang et al., 2020; Yu et al., 2020a). Implementing the freeze-thaw process (hereafter STEMMUS-FT, for applications in cold regions), it facilitates our understanding of the hydrothermal dynamics of respective components in frozen soil medium (i.e., soil liquid water, water vapor, dry air, and ice) (Yu et al., 2018; Yu et al., 2020b; see Section S2).

S1.2 Snowpack module

The Utah energy balance (UEB) snowpack model (Tarboton and Luce, 1996) is a single-layer physically based snow accumulation and melt model. The snowpack is characterized as the conservation of mass and energy using two primary state variables, snow water equivalent W_{SWE} and the internal energy U (see Section S3). Snowpack temperature is expressed diagnostically as the function of W_{SWE} and U, together with the states of snowpack (i.e., solid, solid and liquid mixture, and liquid). Given the insulation effect of the snowpack, snow surface temperature differs from the snowpack bulk temperature, which is mathematically considered using the equilibrium method (i.e., balances energy fluxes at the snow surface). The age of the snow surface, as the auxiliary state variable, is utilized to calculate snow albedo (see Section S3.2.4). The melt outflow is calculated using Darcy's law with the liquid fraction as inputs.

UEB is recognized as one simple yet physically based snowmelt model, which can capture the first order snow process (e.g., diurnal variation of meltwater outflow rate, snow accumulation, and ablation, see a general overview of UEB model development and applications in Table S6.3). It requires little effort in parameter calibration and can be easily transportable and applicable to various locations (e.g., Gardiner et al., 1998; Schulz and de Jong, 2004; Watson et al., 2006; Sultana et al., 2014; Pimentel et al., 2015; Gichamo and Tarboton, 2019) especially for data scarce regions as for example Tibetan Plateau.

S1.3 Structures

In the following sections, STEMMUS-FT module, including its governing equations, constitutive equations, underlying physics, and the difference among three level of model complexities, is first introduced in Section S2. The description of snowmelt module UEB is followed by in Section S3. Section S4 presents the coupling procedure of STEMMUS-UEB model and its structure, subroutines and input data. The following Section S5 shows the model capability in understanding the water and heat transfer mechanisms in frozen soils. Section S6 presents the supplemental tables and figures.

S2 STEMMUS-FT model

The STEMMUS (Simultaneous Transfer of Energy, Momentum and Mass in Unsaturated Soil), detailed in (Zeng et al., 2011b, a; Zeng and Su, 2013), taking into account the soil Freeze-Thaw process (STEMMUS-FT, Yu et al., 2018) was developed. Three levels of complexity of mass and heat transfer physics are made available in the current STEMMUS-FT modelling framework (Yu et al., 2020b). First, the 1-D Richards equation and heat conduction were deployed in STEMMUS-FT to describe the isothermal water flow and heat flow (termed BCD). In the BCD model, the interaction of soil water and heat transfer is only implicitly via the parameterization of heat capacity, thermal conductivity and the water phase change effect. For the advanced coupled water and heat transfer (ACD model), the water flow is affected by soil temperature regimes. The movement of water vapor, as the linkage between soil water and heat flow, is explicitly characterized. STEMMUS-FT further enables the simulation of temporal dynamics of three water phases

(liquid, vapor and ice), together with the soil dry air component (termed ACD-Air model).

In the following sections, we first present the governing equations, underlying physics, and constitutive equations of liquid water flow, vapor flow, air flow, and heat flow for the complete STEMMUS-FT (ACD-Air) model in Section S2.1 and S2.2. The description of BCD, ACD model and the different physics among three levels of model complexities are given in Section S2.3.

S2.1 Governing Equations

S2.1.1 Soil water transfer

$$\frac{\partial}{\partial t}(\rho_L\theta_L + \rho_V\theta_V + \rho_i\theta_i) = -\frac{\partial}{\partial z}(q_{Lh} + q_{LT} + q_{La} + q_{Vh} + q_{VT} + q_{Va}) - S$$
$$= \rho_L\frac{\partial}{\partial z}\left[K\left(\frac{\partial h}{\partial z} + 1\right) + D_{TD}\frac{\partial T}{\partial z} + \frac{K}{\gamma_w}\frac{\partial P_g}{\partial z}\right] + \frac{\partial}{\partial z}\left[D_{Vh}\frac{\partial h}{\partial z} + D_{VT}\frac{\partial T}{\partial z} + D_{Va}\frac{\partial P_g}{\partial z}\right] - S \quad \text{(S2.1)}$$

where $\rho_{L,}$ ρ_V and ρ_i (kg m^{-3}) are the density of liquid water, water vapor and ice, respectively; θ_L, θ_V and θ_i (m^3 m^{-3}) are the volumetric water content (liquid, vapor and ice, respectively); z (m) is the vertical space coordinate (positive upwards); S (s^{-1}) is the sink term for the root water extraction. K (m s^{-1}) is hydraulic conductivity; h (m) is the pressure head; T (°C) is the soil temperature; and P_g (Pa) is the mixed pore-air pressure. γ_W (kg m^{-2} s^{-2}) is the specific weight of water. D_{TD} (kg m^{-1} s^{-1} °C^{-1}) is the transport coefficient for adsorbed liquid flow due to temperature gradient; D_{Vh} (kg m^{-2} s^{-1}) is the isothermal vapor conductivity; and D_{VT} (kg m^{-1} s^{-1} °C^{-1}) is the thermal vapor diffusion coefficient. D_{Va} is the advective vapor transfer coefficient (Zeng et al., 2011b, a). q_{Lh}, q_{LT}, and q_{La}, (kg m^{-2} s^{-1}) are the liquid water fluxes driven by the gradient of matric potential $\frac{\partial h}{\partial z}$, temperature $\frac{\partial T}{\partial z}$, and air pressure $\frac{\partial P_g}{\partial z}$, respectively. q_{Vh}, q_{VT}, and q_{Va} (kg m^{-2} s^{-1}) are the water vapor fluxes driven by the gradient of matric potential $\frac{\partial h}{\partial z}$, temperature $\frac{\partial T}{\partial z}$, and air pressure $\frac{\partial P_g}{\partial z}$, respectively.

S2.1.2 Dry air transfer

$$\frac{\partial}{\partial t}[\varepsilon\rho_{da}(S_a + H_cS_L)] = \frac{\partial}{\partial z}\left[D_e\frac{\partial\rho_{da}}{\partial z} + \rho_{da}\frac{S_aK_g}{\mu_a}\frac{\partial P_g}{\partial z} - H_c\rho_{da}\frac{q_L}{\rho_L} + \left(\theta_aD_{Vg}\right)\frac{\partial\rho_{da}}{\partial z}\right] \quad \text{(S2.2)}$$

where ε is the porosity; ρ_{da} (kg m^{-3}) is the density of dry air; S_a (=1-S_L) is the degree of air saturation in the soil; S_L (=θ_L/ε) is the degree of saturation in the soil; H_c is Henry's constant; D_e (m^2 s^{-1}) is the molecular diffusivity of water vapor in soil; K_g (m^2) is the intrinsic air permeability; μ_a (kg m^{-2} s^{-1}) is the air viscosity; q_L (kg m^{-2} s^{-1}) is the liquid water flux; θ_a (=θ_V) is the volumetric fraction of dry air in the soil; and D_{Vg} (m^2 s^{-1}) is the gas phase longitudinal dispersion coefficient (Zeng et al., 2011a, b).

S2.1.3 Energy transfer

$$\frac{\partial}{\partial t}\left[(\rho_s\theta_sC_s + \rho_L\theta_LC_L + \rho_V\theta_VC_V + \rho_{da}\theta_aC_a + \rho_i\theta_iC_i)(T - T_r) + \rho_V\theta_VL_0 - \rho_i\theta_iL_f\right] - \rho_LW\frac{\partial\theta_L}{\partial t} \quad \text{(S2.3)}$$

$$= \frac{\partial}{\partial z}\left(\lambda_{eff}\frac{\partial T}{\partial z}\right) - \frac{\partial}{\partial z}[q_L C_L(T-T_r) + q_V(L_0 + C_V(T-T_r)) + q_a C_a(T-T_r)] - C_L S(T-T_r)$$

where C_s, C_L, C_V, C_a and C_i (J kg^{-1} °C^{-1}) are the specific heat capacities of solids, liquid, water vapor, dry air and ice, respectively; ρ_s (kg m^{-3}) is the density of solids; $\theta_s$is the volumetric fraction of solids in the soil; T_r (°C) is the reference temperature; L_0 (J kg^{-1}) is the latent heat of vaporization of water at temperature T_r; L_f (J kg^{-1}) is the latent heat of fusion; W (J kg^{-1}) is the differential heat of wetting (the amount of heat released when a small amount of free water is added to the soil matrix); and λ_{eff} (W m^{-1} °C^{-1}) is the effective thermal conductivity of the soil; q_L, q_V, and q_a (kg m^{-2} s^{-1}) are the liquid, vapor water flux and dry air flux.

S2.1.4 Underlying physics and calculation procedure

1) Underlying physics of STEMMUS-FT

When soil water starts freezing, soil liquid water, ice, vapor, and gas coexist in soil pores. A new thermodynamic equilibrium system will be reached and can be described by the Clausius Clapeyron equation (Fig. S2.1). In combination with soil freezing characteristic curve (SFCC), the storage variation of soil water can be partitioned into the variation of liquid water content θ_L and ice content θ_i, and then vapor content θ_V.

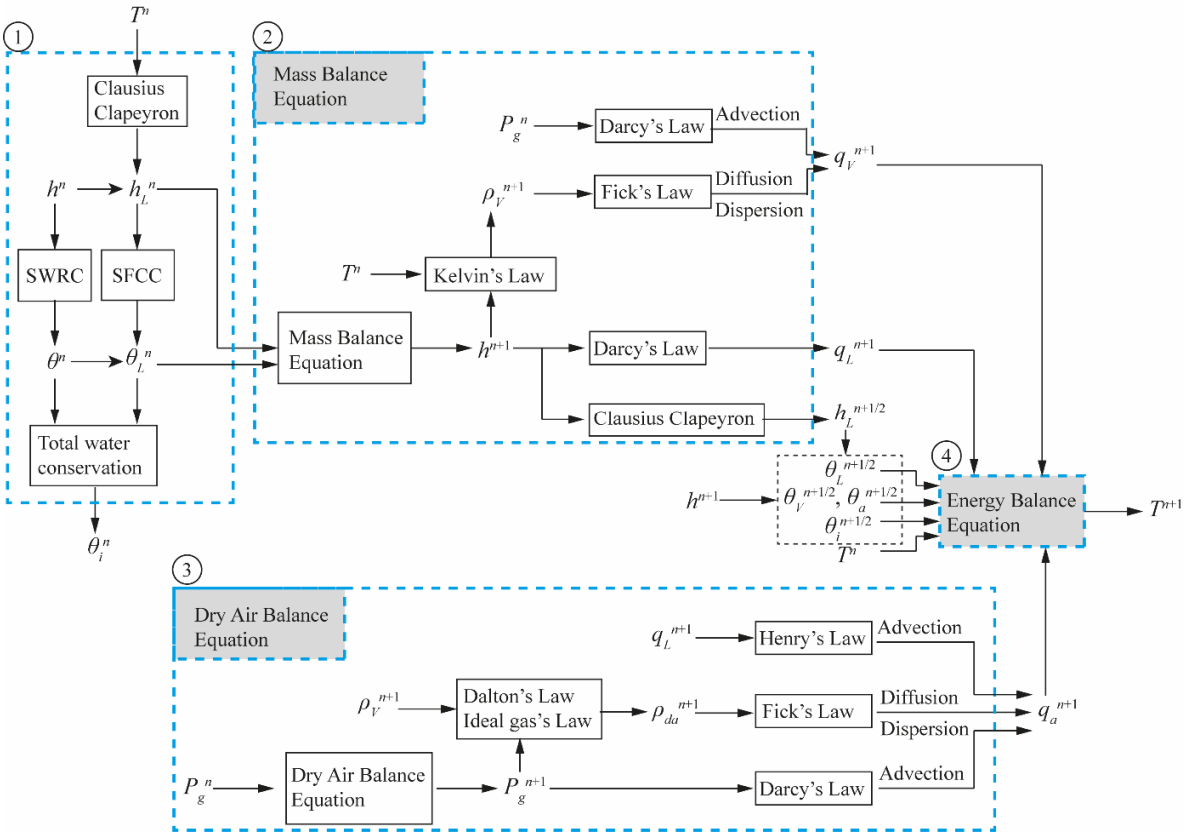

Figure S2.1. The underlying physics and calculation procedure of STEMMUS-FT expressed within one time step. n is the time at the beginning of the time step, n+1 is the time at the end. The variables with the superscript (n+1/2) are the intermediate values.

With regard to a unit volume of soil, the change of water mass storage with time can be attributed to the change of liquid/vapor fluxes and the root water uptake S (Eq. S2.1). The fluxes, in the right-hand side of Eq. S2.1, can be generalized as the sum of liquid and vapor fluxes. The liquid water transfer is expressed by a general form of Darcy's flow $(-\rho_L K \frac{\partial\left(h+\frac{P_g}{\gamma_w}+z\right)}{\partial z})$. According to Kay and Groenevelt (1974), the other source of liquid flow is induced by the effect of the heat of wetting on the pressure field $(-\rho_L D_{TD} \frac{\partial T}{\partial z})$.

The vapor flow is assumed to be induced in three ways: i) the diffusive transfer (Fick's law), driven by a vapor pressure gradient $(-D_V \frac{\partial \rho_V}{\partial z})$. ii) the dispersive transfer due to the longitudinal dispersivity (Fick's law, $-\theta_V D_{Vg} \frac{\partial \rho_V}{\partial z}$). iii) the advective transfer, as part of the bulk flow of air $(\rho_V \frac{q_a}{\rho_{da}})$. As the vapor density is a function of temperature T and matric potential h (Kelvin's law, Eq. S2.18), the diffusive and dispersive vapor flux can be further partitioned into isothermal vapor flux, driven by the matric potential gradient $(D_{Vh} \frac{\partial h}{\partial z})$, and the thermal vapor flux, driven by the temperature gradient $(D_{VT} \frac{\partial T}{\partial z})$. The advective vapor flux, driven by the air pressure gradient, can be expressed as $(D_{Va} \frac{\partial P_g}{\partial z})$ in Equation S2.1.

Dry air transfer in soil includes four components (Eq. S2.2): 1) the diffusive flux (Fick's law) $D_e \frac{\partial \rho_{da}}{\partial z}$, driven by dry air density gradient; 2) the advective flux (Darcy's law,$\rho_{da} \frac{S_a K_g}{\mu_a} \frac{\partial P_g}{\partial z}$), driven by the air pressure gradient; 3) the dispersive flux (Fick's law, $\left(\theta_a D_{Vg}\right) \frac{\partial \rho_{da}}{\partial z}$); and 4) the advective flux due to the dissolved air (Henry's law, $H_c \rho_{da} \frac{q_L}{\rho_L}$). According to Dalton's law of partial pressure, the mix soil air pressure P_g is the sum of the dry air pressure and water vapor pressure. Considering dry air as an ideal gas, the dry air density ρ_{da}, can be expressed as the function of air pressure P_g, water vapor density ρ_V, thus the function of three state variables (h, T, P_g) (see Eqs. S2.20 & S2.21).

Heat transfer in soils includes conduction and convection. The conductive heat transfer contains contributions from liquid, solid, gas and ice $(\lambda_{eff} \frac{\partial T}{\partial z})$. The convective heat is transferred by liquid flux $-C_L q_L (T - T_r)$, $-C_L S (T - T_r)$, vapor flux $-[L_0 q_V + C_V q_V (T - T_r)]$ and air flow $q_a C_a (T - T_r)$. The heat storage in soil, the left hand side of Equation S2.3, includes the bulk volumetric heat content $(\rho_s \theta_s C_s + \rho_L \theta_L C_L + \rho_V \theta_V C_V + \rho_i \theta_i C_i)(T - T_r)$, the latent heat of vaporization $(\rho_V \theta_V L_0)$, the latent heat of freezing/thawing $(-\rho_i \theta_i L_f)$ and a source term associated with the exothermic process of wetting of a porous medium (integral heat of wetting) $(-\rho_L W \frac{\partial \theta_L}{\partial t})$.

2) Calculation procedure of STEMMUS-FT

The mutual dependence of soil temperature and water content makes frozen soils a complicated thermodynamic equilibrium system. The freezing effect explicitly considered in STEMMUS-FT includes three parts: i) the blocking effect on conductivities (see Eq. S2.11); ii) thermal effect on soil thermal capacity/conductivity (see Section S2.2.8); iii) the release/absorption of latent heat flux during water phase change. The calculation procedure of STEMMUS-FT can be summarized as Fig. S2.1.

Step 1. Partition of the soil mass storage

Firstly, applying the Clausius Clapeyron equation, soil temperature T at time step n was utilized to achieve the initial soil freezing water potential. Given the pre-freezing water matric potential h and liquid water matric potential h_L, the SFCC and SWRC are applied to obtain pre-freezing water content θ and liquid water content θ_L . Then the soil ice content θ_i can be derived via total water conservation equation considering the difference in the density between liquid and ice water. The volumetric fraction of soil vapor θ_V in soil pores is the difference of soil porosity and the total water content.

Step 2. Solving the mass balance equation

Taking the soil mass storage variables and matric potentials as inputs, we can solve the mass balance equation successfully. Then a new matric potential can be achieved. Applying Darcy's law with consideration of the blocking effect of soil ice on the hydraulic conductivity, we can get liquid water flux q_L. The liquid water matric potential can be updated by applying Clausius Clapeyron equation. Applying the Kelvin's law (Eq. S2.18), we can update the vapor density ρ_V at the end of time step. Then the dispersive and diffusive vapor flux are possible to be calculated according to Fick's law. Another component of vapor flux is considered as part of the bulk flow of air, which is driven by the air pressure according to Darcy's law.

Step 3. Solving the dry air balance equation

When considering soil dry air as an independent component in soil pores, the dry air balance equation is utilized, whose solution provides the new air pressure P_g^{n+1}. Applying Dalton's law, air pressure can be partitioned into vapor pressure and dry air pressure. Given the updated vapor density, the dry air density can be expressed as the function of air pressure, and vapor density (Eqs. S2.20 & S2.21). Applying Fick's law, we can calculate the diffusive and dispersive components of dry air flux. Applying Darcy's law, the advective flux is derived from the air pressure. To maintain the mechanical and chemical equilibrium, a certain amount of air will dissolve into liquid, such effect is described by Henry's law. Finally, we can achieve the dry air flux q_a by the sum of the aforementioned effects.

Step 4. Solving the energy balance equation

Given the inputs, updated values of liquid water flux q_L^{n+1}, water vapor flux q_V^{n+1}, soil liquid water content $\theta_L^{n+1/2}$, vapor content $\theta_V^{n+1/2}$, ice content $\theta_i^{n+1/2}$, and dry air flux q_a^{n+1}, we can update the thermal parameters, calculate the latent heat of water phase change, then solve the energy balance equation. A successful estimate of soil temperature will be obtained, which can be used as inputs for the next time step.

S2.2 Constitutive Equations

S2.2.1 Unfrozen water content

As the fixed freezing point methods is not physically realistic, the freezing point depression theory was employed in deriving the soil freezing characteristic curve (SFCC) for estimating the unfrozen water content (Koopmans and Miller, 1966; Dall'Amico, 2010). In combination with Clapeyron equation and two soil water retention curve models, two different kinds of SFCC are given below.

Clapeyron + Van Genucthen (Van Genuchten, 1980)

$$\theta_{tot}(h) = \begin{cases} \theta_r + \frac{\theta_s - \theta_r}{[1+|\alpha h|^n]^m}, & h < 0 \\ \theta_s, & h \geq 0 \end{cases}, \quad \text{(S2.4)}$$

where α is related to the inverse air-entry pressure. θ_{tot}, θ_s, and θ_r are the total water content, saturated water content and the residual water content, respectively; h (m) is the pre-freezing soil water potential; m is the empirical parameter. The parameter m is a measure of the pore-size distribution and can be expressed as m = 1-1/n, which in turn can be determined by fitting van Genuchten's analytical model (Van Genuchten, 1980).

The unfrozen water content was estimated by employing soil freezing characteristic curve (SFCC) (Dall'Amico, 2010)

$$\theta_L(h,T) = \theta_r + \frac{\theta_s - \theta_r}{[1+|\alpha(h+h_{Frz})|^n]^m}, \quad \text{(S2.5)}$$

where θ_L is the liquid water content, L_f (J kg^{-1}) is the latent heat of fusion, g (m s^{-2}) is the gravity acceleration, T_0 (273.15 ºC) is the absolute temperature. h (m) is the pre-freezing pressure and α, n, and m are the van Genuchten fitting parameters. h_{Frz} (m) is the soil freezing potential.

$$h_{Frz} = \frac{L_f}{gT_0}(T - T_0) \cdot H(T - T_{CRIT}), \quad \text{(S2.6)}$$

where T (ºC) is the soil temperature. H is the Heaviside function, whose value is zero for negative argument and one for positive argument, T_{CRIT} (ºC) is the soil freezing temperature.

$$T_{CRIT} = T_0 + \frac{ghT_0}{L_f}, \quad \text{(S2.7)}$$

Clapeyron + Clapp and Hornberger (Clapp and Hornberger, 1978)

$$\theta_L(h,T) = \theta_s\left(\frac{L_f}{g\psi_s}\frac{T-T_f}{T}\right)^{-1/b}, \quad \text{(S2.8)}$$

where ψ_s (m) is the air-entry pore water potential, b is the empirical Clapp and Hornberger parameter.

S2.2.2 Hydraulic conductivity

According to the pore-size distribution model (Mualem, 1976), the unsaturated hydraulic conductivity using Clapp and Hornberger, van Genuchten method can be expressed as,

$$K_{Lh} = K_s(\theta/\theta_s)^{3+2/\beta}, \quad \text{(S2.9)}$$

$$K_{Lh} = K_s S_e^l[1 - (1 - S_e^{1/m})^m]^2, \quad \text{(S2.10a)}$$

$$S_e = \frac{\theta - \theta_r}{\theta_s - \theta_r}, \quad \text{(S2.10b)}$$

$$m = 1 - 1/n, \quad \text{(S2.10c)}$$

where K_{Lh} and K_s (m s^{-1}) are the hydraulic conductivity and saturated hydraulic conductivity. $\beta(= 1/b)$ is the empirical Clapp and Hornberger parameter. S_e is the effective saturation. l, n, and m are the van Genuchten fitting parameters.

The block effect of the ice presence in soil pores on the hydraulic conductivity is generally characterized by a correction coefficient, which is a function of ice content (Taylor and Luthin, 1978; Hansson et al., 2004),

$$K_{fLh} = 10^{-EQ} K_{Lh}, \quad \text{(S2.11a)}$$

$$Q = (\rho_i \theta_i / \rho_L \theta_L), \quad \text{(S2.11b)}$$

where K_{fLh} (m s^{-1}) is the hydraulic conductivity in frozen soils, K_{Lh} (m s^{-1}) is the hydraulic conductivity in unfrozen soils at the same negative pressure or liquid moisture content, Q is the mass ratio of ice to total water, and E is the empirical constant that accounts for the reduction in permeability due to the formation of ice (Hansson et al., 2004).

S2.2.3 Temperature dependence of matric potential and hydraulic conductivity

Soil matric potential and hydraulic conductivity are dependent on soil temperature in STEMMUS (Zeng and Su, 2013), which is related to soil water surface tension and viscous flow effects. The temperature dependence of matric potential can be expressed as

$$h_{Cor\_T} = he^{-C_\psi (T - T_r)} \quad \text{(S2.12)}$$

where, h_{Cor_T} is the soil matric potential considering temperature effect; C_ψ is the temperature coefficient, assumed to be constant as 0.0068 ^{o}C^{-1} (Milly, 1982); T_r is the reference temperature (20 ^{o}C).
Hydraulic conductivity, taken into account the temperature effect, can be written as

$$K(\theta, T) = K_s K_r(\theta) K_T(T) \quad \text{(S2.13)}$$

where $K_r(\theta)$ is the relative hydraulic conductivity, $K_T(T)$ is the temperature coefficient of hydraulic conductivity, expressed as

$$K_T(T) = \frac{\mu_w(T_r)}{\mu_w(T)} \quad \text{(S2.14)}$$

where μ_w is the viscosity of water. The dynamic viscosity of water can be written as

$$\mu_w(T) = \mu_{w0} \exp\left[\frac{\mu_1}{R(T + 133.3)}\right] \quad \text{(S2.15)}$$

where μ_{w0} is the water viscosity at reference temperature, μ_1=4.7428 (kJ mol^{-1}), R =8.314472 (J mol^{-1} ^{o}C^{-1}), T is temperature in ^{o}C.

S2.2.4 Gas conductivity

According to Darcy's law, the gas conductivity can be expressed as

$$K_g = \frac{K_{rg}(S_a) K_s \mu_w}{\rho_L g \mu_g} \quad \text{(S2.16)}$$

where μ_g is gas viscosity, and the air viscosity; K_{rg} is the relative gas conductivity, which is a function of effective gas saturation and is defined by Van Genuchten-Mualem model,

$$K_{rg} = (1 - S_a^{0.5})[1 - (1 - (1 - S_a)^{\frac{1}{m}})^m]^2 \quad \text{(S2.17)}$$

S2.2.5 Gas phase density

The gas in the soil pores includes water vapor and dry air. The water vapor density, according to Kelvin's law, is expressed as (Philip and Vries, 1957)

$$\rho_V = \rho_{sV} H_r, \quad H_r = \exp\left(\frac{hg}{R_V T}\right), \tag{S2.18}$$

where ρ_{sV} is the density of saturated water vapor; H_r is the relative humidity; R_V (461.5 J kg^{-1} K^{-1}) is the specific gas constant for vapor; g is the gravitation acceleration; T is temperature.

The gradient of the water vapor density with respect to z can be expressed as

$$\frac{\partial \rho_V}{\partial z} = \rho_{sV} \frac{\partial H_r}{\partial T}\Big|_h + \rho_{sV} \frac{\partial H_r}{\partial h}\Big|_T + H_r \frac{\partial \rho_V}{\partial T}\frac{\partial T}{\partial z}, \tag{S2.19}$$

Assuming that the pore-air and pore-vapor could be considered as ideal gas, then soil dry air and vapor density can be given as

$$\rho_{da} = \frac{P_{da}}{R_{da} T}, \quad \rho_V = \frac{P_V}{R_V T}, \tag{S2.20}$$

where R_{da} (287.1J kg^{-1} K^{-1}) is the specific gas constant for dry air; P_{da} and P_V (Pa) are the dry air pressure and vapor pressure. Following Dalton's law of partial pressure, the mixed soil air pressure is the sum of the dry air pressure and the vapor pressure, i.e., $P_g = P_{da} + P_V$. Thus, combining with Eq. S2.20, the soil dry air density can be derived as

$$\rho_{da} = \frac{P_g}{R_{da} T} - \frac{\rho_V R_V}{R_{da}}, \tag{S2.21}$$

The derivation of dry air density with respect to time and space are

$$\frac{\partial \rho_{da}}{\partial t} = X_{aa} \frac{\partial P_g}{\partial t} + X_{aT} \frac{\partial T}{\partial t} + X_{ah} \frac{\partial h}{\partial t}, \tag{S2.22}$$

$$\frac{\partial \rho_{da}}{\partial z} = X_{aa} \frac{\partial P_g}{\partial z} + X_{aT} \frac{\partial T}{\partial z} + X_{ah} \frac{\partial h}{\partial z}, \tag{S2.23}$$

where

$$X_{aa} = \frac{1}{R_{da} T}, \tag{S2.24}$$

$$X_{aT} = \left[\frac{P_g}{R_{da} T^2} + \frac{R_V}{R_{da}}\left(H_r \frac{\partial \rho_{sV}}{\partial T} + \rho_{sV} \frac{\partial H_r}{\partial T}\right)\right], \tag{S2.25}$$

$$X_{ah} = -\frac{\partial \rho_V}{\partial h}, \tag{S2.26}$$

S2.2.6 Vapor diffusivity

The isothermal vapor diffusivity is followed the simple theory and expressed as

$$D_{V\_Iso} = D_V \frac{\partial \rho_V}{\partial h} = D_{atm} \nu \tau \theta_a \frac{\partial \rho_V}{\partial h}, \tag{S2.27}$$

where ν is set to 1, $\tau = \theta_a^{2/3}$, and $D_{atm} = 0.229\left(1 + \frac{T}{273}\right)^{1.75}$ (m^2 s^{-1}).

The thermal vapor diffusivity is given by considering the enhancement factor as

$$D_{V\_NonIso} = D_V \frac{\partial \rho_V}{\partial T} = D_{atm} \eta \frac{\partial \rho_V}{\partial T}, \tag{S2.28}$$

where η is the thermal enhancement factor.

S2.2.7 Gas dispersivity

According to Bear, the gas phase longitudinal dispersivity *D*vg is expressed as

$$D_{Vg} = \alpha_{L\_i} q_i, \quad i = gas\ or\ liquid, \tag{S2.29}$$

where q_i is the pore fluid flux in phase i, and α_{L_i} is the longitudinal dispersivity in phase *i*, which can be related to the soil saturation as

$$\alpha_{L\_i} = \alpha_{L\_Sat}\left[13.6 - 16 \times \frac{\theta_g}{\epsilon} + 3.4 \times \left(\frac{\theta_g}{\epsilon}\right)^5\right], \tag{S2.30}$$

Following Grifoll's work, the saturation dispersivity can be set to 0.078 m in case of lacking dispersivity values.

S2.2.8 Thermal properties

1) Heat capacity

The volumetric heat capacity is the average of the soil component capacity weighted by its fraction.

$$C = \sum_{i=1}^{6} C_j \theta_j \tag{S2.31}$$

where C_j and θ_j are the volumetric heat capacity and volumetric fraction of the *j*th soil constituent (J cm-3 ° C-1). The components are (1) water, (2) air, (3) quartz particles, (4) other minerals, (5) organic matter, and (6) ice (see Table S2.1).

2) Thermal Conductivity

The method used to calculate the frozen soil heat conductivity can be divided into three categories: i) empirical method (e.g., Campbell method as used in Hansson et al., 2004), ii) Johansen method (Johansen, 1975), and iii) de Vires method (de Vries, 1963). Due to the necessity in the calibration of parameters, the empirical Campbell method is not easy to adapt and rarely employed in LSMs and thus not discussed in the current context. The other variations of Johansen method and de Vries method, in which the parameters are based on soil texture information, i.e., Farouki method (Farouki, 1981) and the simplified de Vries method (Tian et al., 2016), were further incorporated into STEMMUS-FT.

Johansen method (Johansen, 1975)

The soil thermal conductivity is the weighted function of soil dry and saturated thermal conductivity,

$$\lambda_{eff} = K_e\left(\lambda_{sat} - \lambda_{dry}\right) + \lambda_{dry}, \tag{S2.32}$$

where the λ_{sat} (W m^{-1} °C^{-1}) is saturated thermal conductivity, λ_{dry} (W m^{-1} °C^{-1}) is the dry thermal conductivity, K_e is the Kersten number, which can be expressed as

$$K_{\mathrm{e}} = \begin{cases} \log\left(\theta/\theta_s\right) + 1.0, & \theta/\theta_s > 0.05 \\ 0.7\log\left(\frac{\theta}{\theta_s}\right) + 1.0, & \theta/\theta_s > 0.1 \\ \theta/\theta_s, & frozen\ soil \end{cases}, \tag{S2.33}$$

The saturated thermal conductivity λ_{sat} is the weighted value of its components (soil particles λ_{soil} and water λ_{w}),

$$\lambda_{\mathrm{sat}} = \lambda_{\mathrm{soil}}^{1-\theta_s}\lambda_w^{\theta_s}, \tag{S2.34}$$

where the solid soil thermal conductivity λ_{soil} can be described as

$$\lambda_{\mathrm{soil}} = \lambda_{\mathrm{qtz}}^{\mathrm{qtz}}\lambda_{\mathrm{o}}^{1-\mathrm{qtz}}, \tag{S2.35}$$

where the λ_{qtz} and λ_{o} (W m^{-1} °C^{-1}) are the thermal conductivity of the quartz and other soil particles, qtz is the volumetric quartz fraction.

The dry soil thermal conductivity is a function of dry soil density ρ_d,

$$\lambda_{dry} = \frac{0.135\rho_d + 64.7}{2700 - 0.947\rho_d}, \tag{S2.36}$$

$$\rho_d = (1-\theta_s)\cdot 2700, \tag{S2.37}$$

Farouki method (Farouki, 1981)

Similar to Johansen method, the weighted method between the saturated and dry thermal conductivities is utilized by Farouki method to estimate soil thermal conductivity. The difference between Farouki method and Johansen method is to express the dry thermal conductivity and solid soil thermal conductivity as the function of soil texture. Equation S2.35 can be replaced with,

$$\lambda_{\mathrm{soil}} = \frac{8.80\cdot(\%\mathrm{sand}) + 2.92\cdot(\%\mathrm{clay})}{(\%\mathrm{sand}) + (\%\mathrm{clay})}, \tag{S2.38}$$

where %sand, %clay are the volumetric fraction of sand and clay.

de Vires method (de Vries, 1963)

$$\lambda_{eff} = \left(\sum_{j=1}^{6} k_j\theta_j\lambda_{\mathrm{j}}\right)\left(\sum_{j=1}^{6} k_j\theta_j\right)^{-1}, \tag{S2.39}$$

where k_j is the weighting factor for each components; θ_j the volumetric fraction of the *j*th constituent; λ_{j} (W m^{-1} °C^{-1}) the thermal conductivity of the *j*th constituent. The six components are: 1. water, 2. air, 3. quartz particles, 4. clay minerals, and 5.organic matter, 6, ice. (see Table S2.1).

$$k_j = \frac{2}{3}\left[1 + \left(\frac{\lambda_{\mathrm{j}}}{\lambda_1} - 1\right)g_{\mathrm{j}}\right]^{-1} + \frac{1}{3}\left[1 + \left(\frac{\lambda_{\mathrm{j}}}{\lambda_1} - 1\right)(1 - 2g_{\mathrm{j}})\right]^{-1}, \tag{S2.40}$$

and g_{j} is the shape factor of the *j*th constituent (see Table S2.1), of which the shape factor of the air g_2 can be determined as follows,

$$g_2 = \begin{cases} 0.013 + \left(\frac{0.022}{\theta_{wilting}} + \frac{0.298}{\theta_s}\right)\theta_L, & \theta_L < \theta_{wilting} \\ 0.035 + \frac{0.298}{\theta_s}\theta_L, & \theta_L \geq \theta_{wilting} \end{cases}, \tag{S2.41}$$

Table S2.1 Properties of Soil Constituents (de Vries, 1963)

Substance	*j*	λ_j (mcal cm^{-1} s^{-1} °C^{-1})	C_j (mcal cm^{-1} s^{-1} °C^{-1})	ρ_j (g cm^{-3})	g_j
Water	1	1.37	1	1	…
Air	2	0.06	0.0003	0.00125	…
Quartz	3	21	0.48	2.66	0.125
Clay minerals	4	7	0.48	2.65	0.125
Organic matter	5	0.6	0.6	1.3	0.5
Ice	6	5.2	0.45	0.92	0.125

Simplified de Vries model (Tian et al., 2016)

Tian et al. (2016) proposed the simplified de Vries method as an alternative method of traditional de Vries method. In this method, the thermal conductivity of soil particles component can be directly estimated based on the relative contribution of measured soil constitutes.

$$\lambda_{eff} = \frac{\theta_w\lambda_w + k_i\theta_i\lambda_i + k_a\theta_a\lambda_a + k_{min}\theta_{min}\lambda_{min}}{\theta_w + k_i\theta_i + k_a\theta_a + k_{min}\theta_{min}}, \quad \text{(S2.42)}$$

where k_{min} , can be derived by Eq. S2.40, is the weighting factor of soil minerals, θ_{min} is the volumetric fraction of soil minerals, λ_{min} (W m^{-1} °C^{-1}) is the thermal conductivity of soil minerals, can be expressed as the weighted value of its components,

$$\lambda_{min} = \lambda_{sand}^{f_{sand}}\lambda_{silt}^{f_{silt}}\lambda_{clay}^{f_{clay}}, \quad \text{(S2.43)}$$

where f_{sand}, f_{silt}, and f_{clay} are the volumetric fraction of soil sand, silt and clay, respectively. The shape factor of soil minerals is determined as the volumetrically weighted arithmetic mean of the constituent shape factors,

$$g_{a,min} = g_{a,sand}f_{sand} + g_{a,silt}f_{silt} + g_{a,clay}f_{clay}, \quad \text{(S2.44)}$$

where $g_{a,sand}$, $g_{a,silt}$, $g_{a,clay}$ are the shape factors of soil sand, silt and clay, their values are 0.182, 0.0534 and 0.00775, respectively (Tarnawski and Wagner, 1992; Tarnawski and Wagner, 1993; Tian et al., 2016).

3) Differential Heat of Wetting

The differential heat of wetting, W is the amount of heat released when a small amount of free water is added to the soil matrix and expressed by Edlefsen and Anderson (1943) as

$$\mathrm{W} = -\rho_L\left(\psi - T\frac{\psi}{T}\right) = -0.01g(h + Tah) = -0.01gh(1 + Ta), \quad \text{(S2.45)}$$

where Prunty (2002) expressed the differential heat of wetting as

$$\mathrm{W} = -0.2932h, \quad \text{(S2.46)}$$

4) Transport coefficient for adsorbed liquid flow

The transport coefficient for adsorbed liquid flow due to temperature gradient is expressed as Groenevelt and Kay (1974)

$$D_{Ta} = \frac{H_w\epsilon}{b\tau\mu_w T}(1.5548 \times 10^{-15}), \quad \text{(S2.47)}$$

where H_w is the integral heat of wetting (J m-2); b = 4e-8 (m); T is temperature in °C.

S2.2.9 Calculation of surface evapotranspiration

The one step calculation of actual soil evaporation (E_s) and potential transpiration (T_p) is achieved by incorporating canopy minimum surface resistance and actual soil resistance into the Penman-Monteith model (i.e., the ET_{dir} method in Yu et al., 2016). LAI is implicitly used to partition available radiation energy into the radiation reaching the canopy and soil surface.

$$T_p = \frac{\Delta(R_n^c - G) + \rho_a c_p\frac{(e_s - e_a)}{r_a^c}}{\lambda(\Delta + \gamma\left(1 + \frac{r_{c,min}}{r_a^c}\right))} \quad \text{(S2.48)}$$

$$E_s = \frac{\Delta(R_n^s - G) + \rho_a c_p \frac{(e_s - e_a)}{r_a^s}}{\lambda(\Delta + \gamma(1 + \frac{r_s}{r_a^s}))} \quad \text{(S2.49)}$$

where R_n^c and R_n^s (MJ m^{-2} day^{-1}) are the net radiation at the canopy surface and soil surface, respectively; ρ_a (kg m^{-3}) is the air density; c_p (J kg^{-1} K^{-1}) is the specific heat capacity of air; r_a^c and r_a^s (s m^{-1}) are the aerodynamic resistance for canopy surface and soil surface, respectively; $r_{c,min}$ (s m^{-1}) is the minimum canopy surface resistance; and r_s (s m^{-1}) is the soil surface resistance.

The net radiation reaching the soil surface can be calculated using the Beer's law:

$$R_n^s = R_n\, exp(-\tau LAI) \quad \text{(S2.50)}$$

And the net radiation intercepted by the canopy surface is the residual part of total net radiation:

$$R_n^c = R_n(1 - exp(-\tau LAI)) \quad \text{(S2.51)}$$

The minimum canopy surface resistance $r_{c,min}$ is given by:

$$r_{c,min} = r_{l,min}/LAI_{eff} \quad \text{(S2.52)}$$

where $r_{l,min}$ is the minimum leaf stomatal resistance; LAI_{eff} is the effective leaf area index, which considers that generally the upper and sunlit leaves in the canopy actively contribute to the heat and vapor transfer.

The soil surface resistance can be estimated following van de Griend and Owe (1994),

$$\begin{aligned} r_s &= r_{sl} && \theta_1 > \theta_{min}, h_1 > -100000\ cm \\ r_s &= r_{sl} e^{a(\theta_{min} - \theta_1)} && \theta_1 \le \theta_{min}, h_1 > -100000\ cm \\ r_s &= \infty && h_1 \le -100000\ cm \end{aligned} \quad \text{(S2.53)}$$

where r_{sl} (10 s m^{-1}) is the resistance to molecular diffusion of the water surface; a (0.3565) is the fitted parameter; θ_1 is the topsoil water content; θ_{min} is the minimum water content above which soil is able to deliver vapor at a potential rate.

The root water uptake term described by Feddes et al. (1978) is:

$$S(h) = \alpha(h) S_p \quad \text{(S2.54)}$$

where $\alpha(h)$ (dimensionless) is the reduction coefficient related to soil water potential h; and S_p (s^{-1}) is the potential water uptake rate.

$$S_p = b(z) T_p \quad \text{(S2.55)}$$

where T_p is the potential transpiration in Eq. S2.48. $b(z)$ is the normalized water uptake distribution, which describes the vertical variation of the potential extraction term, S_p, over the root zone. Here the asymptotic function was used to characterize the root distribution as described in (Gale and Grigal, 1987; Jackson et al., 1996; Yang et al., 2009; Zheng et al., 2015).

S2.3 STEMMUS-FT model framework with three levels of complexity

On the basis of STEMMUS modelling framework, the increasing complexity of vadose zone physics in frozen soils was implemented as three alternative models (Table S2.2). Firstly, STEMMUS enabled isothermal water and heat transfer physics (Eqs. S2.56 & S2.57). The 1-D Richards equation is utilized to solve the isothermal water transport in variably saturated soils. The heat conservation equation took into

account the freezing/thawing process and the latent heat due to water phase change. The effect of soil ice on soil hydraulic and thermal properties was considered. It is termed the basic coupled water and heat transfer model (BCD).

Secondly, the fully coupled water and heat physics, i.e., water vapor flow and thermal effect on water flow, was explicitly considered in STEMMUS, termed the advanced coupled model (ACD). For the ACD physics, the extended version of Richards equation (Richards, 1931) with modifications made by Milly (1982) was used as the water conservation equation (Eq. S2.58). Water flow can be expressed as liquid and vapor fluxes driven by both temperature gradients and matric potential gradients. The heat transport in frozen soils mainly includes: heat conduction (CHF, $\lambda_{eff}\frac{\partial T}{\partial z}$), convective heat transferred by liquid flux (HFL, $-C_L q_L(T-T_r)$, $-C_L S(T-T_r)$), vapor flux (HFV, $-C_V q_V(T-T_r)$), the latent heat of vaporization (LHF, $-q_V L_0$), the latent heat of freezing/thawing ($-\rho_i \theta_i L_f$) and a source term associated with the exothermic process of wetting of a porous medium (integral heat of wetting) ($-\rho_L W\frac{\partial \theta_L}{\partial t}$). It can be expressed as Eq. S2.59 (De Vries, 1958; Hansson et al., 2004).

Lastly, STEMMUS expressed the freezing soil porous medium as the mutually dependent system of liquid water, water vapor, ice water, dry air and soil grains, in which other than air flow all other components kept the same as in ACD (termed ACD-Air model) (Eqs. S2.60, S2.61, & S2.62, Zeng et al., 2011a, b; Zeng and Su, 2013). The effects of air flow on soil water and heat transfer can be two-fold. Firstly, the air flow-induced water and vapor fluxes (q_{La}, q_{Va}) and its corresponding convective heat flow (HFa, $-q_a C_a(T-T_r)$) were considered. Secondly, the presence of air flow alters the vapor transfer processes, thus can considerably affects the water and heat transfer in an indirect manner.

STEMMUS-FT utilized the adaptive time-step strategy, with maximum time steps ranging from 1s to 1800s (e.g., with 1800s as the time step under stable conditions). The maximum desirable change of soil moisture and soil temperature within one time step was set as 0.02 $cm^3\ cm^{-3}$ and 2 °C, respectively, to prevent too large change in state variables that may cause numerical instabilities. If the changes between two adjacent soil moisture/temperature states are less than the maximum desirable change, STEMMUS-FT continues without changing the length of current time step (e.g., 1800s). Otherwise, STEMMUS-FT will adjust the time step with a deduction factor, which is proportional to the difference between the too large changes and desirable allowed maximum changes of state variables. Within one single time step, the Picard iteration was used to solve the numerical problem, and the numerical convergence criteria is set as 0.001 for both soil matric potential (in cm) and soil temperature (in °C).

Table S2.2. Governing equations for different complexity of water and heat coupling physics (See Section S4.4 for notations)

Models	Governing equations (water, heat and air)	Number
BCD	$\frac{\partial\theta}{\partial t} = -\frac{\partial q}{\partial z} - S = \rho_L \frac{\partial}{\partial z}\left[K\left(\frac{\partial\psi}{\partial z}+1\right)\right] - S$	(S2.56)
	$\underbrace{C_{soil}\frac{\partial T}{\partial t} - \rho_i L_f \frac{\partial\theta_i}{\partial t}}_{HC} = \frac{\partial}{\partial z}\left(\underbrace{\lambda_{eff}\frac{\partial T}{\partial z}}_{CHF}\right)$	(S2.57)
ACD	$\frac{\partial}{\partial t}(\rho_L\theta_L + \rho_V\theta_V + \rho_i\theta_i) = -\frac{\partial}{\partial z}(q_L + q_V) - S$ $= -\frac{\partial}{\partial z}(q_{Lh} + q_{LT} + q_{Vh} + q_{VT}) - S$ $= \rho_L\frac{\partial}{\partial z}\left[K_{Lh}\left(\frac{\partial\psi}{\partial z}+1\right) + K_{LT}\frac{\partial T}{\partial z}\right] + \frac{\partial}{\partial z}\left[D_{Vh}\frac{\partial\psi}{\partial z} + D_{VT}\frac{\partial T}{\partial z}\right] - S$	(S2.58)
	$\underbrace{\frac{\partial}{\partial t}\left[(\rho_s\theta_s C_s + \rho_L\theta_L C_L + \rho_V\theta_V C_V + \rho_i\theta_i C_i)(T-T_r) + \rho_V\theta_V L_0 - \rho_i\theta_i L_f\right] - \rho_L W\frac{\partial\theta_L}{\partial t}}_{HC}$ $= \frac{\partial}{\partial z}\left(\underbrace{\lambda_{eff}\frac{\partial T}{\partial z}}_{CHF}\right) - \frac{\partial}{\partial z}[\underbrace{q_V L_0}_{LHF} + \underbrace{q_V C_V(T-T_r)}_{HFV}] - \frac{\partial}{\partial z}[\underbrace{q_L C_L(T-T_r)}_{} - \underbrace{C_L S(T-T_r)}_{}]_{HFL}$	(S2.59)
ACD-Air	$\frac{\partial}{\partial t}(\rho_L\theta_L + \rho_V\theta_V + \rho_i\theta_{ice}) = -\frac{\partial}{\partial z}(q_{Lh} + q_{LT} + q_{La} + q_{Vh} + q_{VT} + q_{Va}) - S$ $= \rho_L\frac{\partial}{\partial z}\left[K\left(\frac{\partial\psi}{\partial z}+1\right) + D_{TD}\frac{\partial T}{\partial z} + \frac{K}{\gamma_w}\frac{\partial P_g}{\partial z}\right] + \frac{\partial}{\partial z}\left[D_{Vh}\frac{\partial\psi}{\partial z} + D_{VT}\frac{\partial T}{\partial z} + D_{Va}\frac{\partial P_g}{\partial z}\right] - S$	(S2.60)
	$\underbrace{\frac{\partial}{\partial t}\left[(\rho_s\theta_s C_s + \rho_L\theta_L C_L + \rho_V\theta_V C_V + \rho_{da}\theta_a C_a + \rho_i\theta_i C_i)(T-T_r) + \rho_V\theta_V L_0 - \rho_i\theta_i L_f\right] - \rho_L W\frac{\partial\theta_L}{\partial t}}_{HC}$ $= \frac{\partial}{\partial z}\left(\underbrace{\lambda_{eff}\frac{\partial T}{\partial z}}_{CHF}\right) - \frac{\partial}{\partial z}[\underbrace{q_V L_0}_{LHF} + \underbrace{q_V C_V(T-T_r)}_{HFV} + \underbrace{q_a C_a(T-T_r)}_{HFa}]$ $- \frac{\partial}{\partial z}\underbrace{[q_L C_L(T-T_r)] - C_L S(T-T_r)}_{HFL}$	(S2.61)
	$\frac{\partial}{\partial t}[\varepsilon\rho_{da}(S_a + H_c S_L)] = \frac{\partial}{\partial z}\left[D_e\frac{\partial\rho_{da}}{\partial z} + \rho_{da}\frac{S_a K_g}{\mu_a}\frac{\partial P_g}{\partial z} - H_c\rho_{da}\frac{q_L}{\rho_L} + (\theta_a D_{Vg})\frac{\partial\rho_{da}}{\partial z}\right]$	(S2.62)

The main difference of underlying soil physical processes considered by three level of model complexity is summarized in Table S2.3. For the BCD model, soil water and heat transfer are independent during the unfrozen period, the coupling between water and heat transfer only can be induced by the freezing/thawing process. Such coupling is mainly: i) the ice effect (thermal effect) on soil hydraulic properties; ii) latent heat flux due to phase change. For the ACD model, it enables not only frozen soil physics but also additional processes and most importantly the vapor flow transfer, which links the soil water and heat flow to implement the tight coupling of water and heat effects. In addition to the ice blocking effect as presented in BCD, the thermal effect on water flow is also expressed with the temperature dependence of hydraulic conductivity and matric potential (Section S2.2.3). Furthermore, not only the latent heat due to phase change, but also the convective heat due to liquid/vapor flow can be simulated. For the ACD-Air model, the dry air is considered as an independent component of soil pores and interactively coupled with soil water and heat transfer. The airflow induced convective heat is calculated. Although it contributes little to the total heat budgets while

indeed can affect the relative contribution of other heat flux components (see Section S5.2).

Table S2.3. The underlying soil physical processes considered by STEMMUS-FT with various model complexities

Model complexity	Soil Physical Processes		Model Components
	Unfrozen period	Frozen period	
BCD	Independent water and heat transfer	FT induced water and heat transfer coupling, Ice effect on soil properties, Latent heat due to phase change	Eqs. S2.56 & S2.57
ACD	Tightly coupled water and heat transfer	Tightly coupled water and heat transfer, Ice effect on soil properties, Latent heat due to phase change, Convective heat due to liquid/vapor flow.	Eqs. S2.58 & S2.59
ACD-Air	Tightly coupled water, dry air, and heat transfer	Tightly coupled water, dry air, and heat transfer, Ice effect on soil properties, Latent heat due to phase change, Convective heat due to liquid/vapor/air flow.	Eqs. S2.60 & S2.61 & S2.62

Note:
Independent water and heat transfer: Soil water and heat transfer process is independent.
FT induced water and heat transfer coupling: Soil water and heat transfer process is coupled only during the freezing/thawing (FT) period. Soil water flow is affected by temperature only through the presence of soil ice content (the impedance effect).
Tightly coupled water and heat transfer: Soil water and heat transfer process is tightly coupled; vapor flow, which links the soil water and heat flow, is taken into account; thermal effect on water flow is considered (the hydraulic conductivity and matric potential is dependent on soil temperature; when soil freezes, the hydraulic conductivity is reduced by the presence of soil ice, which is temperature dependent); the convective/advective heat due to liquid/vapor flow can be calculated.
Tightly coupled water, dry air, and heat transfer: On the basis of "Tightly coupled water and heat transfer", the soil dry air transfer is taken into account and simultaneously simulated with water and heat transfer; the convective/advective heat due to liquid/vapor/air flow can be calculated.
Ice effect on soil properties: the explicit simulation of ice content and its effect on the hydraulic/thermal properties.

S3 UEB snowmelt module

The Utah energy balance (UEB) snowmelt model is a physically based snow accumulation and melt model (Fig. S3.1). The snowpack is characterized mainly using two primary state variables, snow water equivalent W and the internal energy U. The snow age is considered as the ancillary state variable. The conservation of mass and energy forms the basis of UEB (Tarboton and Luce, 1996), is presented in Section S3.1. The relevant constitutive equations are given in Section S3.2.

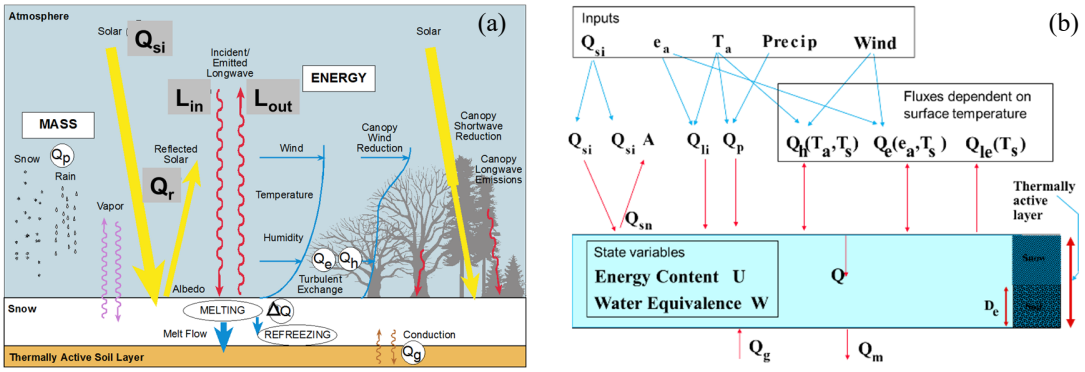

Figure S3.1. The schematic of (a) energy flux involved in snowmelt and snowpack ablation (b) related variables in UEB model. Adapted from Tarboton and Luce (1996).

S3.1 Governing Equations

S3.1.1 Mass balance equation

The increase or decrease of snow water equivalence with time equals the difference of income and outgoing water flux:

$$\frac{dW_{SWE}}{dt} = P_r + P_s - M_r - E \tag{S3.1}$$

where W_{SWE} (m) is the snow water equivalent; P_r (m s^{-1}) is the rainfall rate; P_s (m s^{-1}) is the snowfall rate; M_r (m s^{-1}) is the meltwater outflow from the snowpack; and E (m s^{-1}) is the sublimation from the snowpack.

S3.1.2 Energy balance equation

The energy balance of snowpack can be expressed as:

$$\frac{dU}{dt} = Q_{sn} + Q_{li} + Q_p + Q_g - Q_{le} + Q_h + Q_e - Q_m \tag{S3.2}$$

where Q_{sn} (W m^{-2}) is the net shortwave radiation; Q_{li} (W m^{-2}) is the incoming longwave radiation; Q_p (W m^{-2}) is the advected heat from precipitation; Q_g (W m^{-2}) is the ground heat flux; Q_{le} (W m^{-2}) is the outgoing longwave radiation; Q_h (W m^{-2}) is the sensible heat flux; Q_e (W m^{-2}) is the latent heat flux due to sublimation/condensation; and Q_m (W m^{-2}) is the advected heat removed by meltwater.

Equations S3.1 and S3.2 form a coupled set of first order, nonlinear ordinary differential equations. Euler predictor-corrector approach was employed in UEB model to solve the initial value problems of these equations (Tarboton and Luce, 1996).

S3.2 Constitutive Equations

S3.2.1 Mass balance

The observed precipitation rate P, can be partitioned into rain P_r, and snow P_s, (both in terms of water equivalence depth) based on air temperature T_a

$$\begin{aligned} P_r &= P && T_a \geq T_r \\ P_r &= P(T_a - T_b)/(T_r - T_b) && T_b < T_a < T_r \\ P_r &= 0 && T_a < T_b \end{aligned} \tag{S3.3}$$

$$P_s = F(P - P_r) \tag{S3.4}$$

where T_r is a threshold air temperature above which all precipitation is rain and T_b is a threshold air temperature below which all precipitation is snow. F is employed to account for the wind redistribution effect on the accumulation of snow.

The amount of water sublimate from the snowpack is

$$E = \rho_a(q_s - q_a)K_e \quad \text{(S3.5)}$$

where ρ_a is air density, q_s is the surface specific humidity, q_a is the air humidity. K_e is turbulent transfer conductance for latent heat.

The meltwater outflow from the snowpack can be expressed as

$$M_r = K_{sat}S^{*3} \quad \text{(S3.6)}$$

where K_{sat} is the snow saturated hydraulic conductivity and S^* is the relative saturation in excess of water retained by capillary forces. S^* is given by:

$$S^* = \frac{liquid\ water\ volume - capillary\ retention}{pore\ volume - capillary\ retention} \quad \text{(S3.7)}$$

S3.2.2 Energy balance

The net shortwave radiation is calculated from incident shortwave radiation Q_{si} and albedo α, which is a function of snow age and solar illumination angle.

$$Q_{sn} = (1 - \alpha)Q_{si} \quad \text{(S3.8)}$$

The Stefan–Boltzmann equation is used to estimate the incoming longwave radiation Q_{le} and outgoing longwave radiation Q_{li} based on air temperature T_a and snow surface temperature T_{SS}, respectively.

$$Q_{le} = \varepsilon_s\sigma{T_{SS}}^4 \quad \text{(S3.9)}$$

$$Q_{li} = \varepsilon_a\sigma{T_a}^4 \quad \text{(S3.10)}$$

where ε_s is emissivity of snow, σ is the Stefan Boltzmann constant. ε_a is the air emissivity, which is based on air vapor pressure, air temperature and cloud cover.

The latent heat flux, Q_e and sensible heat flux, Q_h are modeled using bulk aerodynamic formulae:

$$Q_h = \rho_a C_p(T_a - T_{SS})K_h \quad \text{(S3.11)}$$

$$Q_e = \rho_a h_v(q_s - q_a)K_e = K_e\frac{0.622h_v}{R_dT_a}(e_a - e_s(T_{SS})) \quad \text{(S3.12)}$$

K_h and K_e are turbulent transfer conductance for sensible and latent heat respectively. Under neutral atmospheric conditions K_h and K_e can be given by

$$K_e = K_h = \frac{k_v^2 u}{[ln\ (z_m/z_0]^2} \quad \text{(S3.13)}$$

where z_m is the measurement height for wind speed, air temperature, and humidity, u is the wind speed, k_v is von Kármán's constant (0.4), and z_0 is the aerodynamic roughness.

The heat advected with the snow melt outflow, relative to the solid reference state is:

$$Q_m = \rho_w h_f M_r \quad \text{(S3.14)}$$

The advected heat Q_p is the energy required to convert precipitation to the reference state (0 °C ice phase). The temperature of rain and snow is taken as the greater and lesser of the air temperature and freezing point. With different temperature inherent to snow and rain, this amount of energy can be described as

$$Q_p = \rho_w C_s P_s \cdot min(T_a, 0) + P_r\left[\rho_w h_f + \rho_w C_w \cdot max\ (T_a, 0)\right] \quad \text{(S3.15)}$$

S3.2.3 Snow temperatures

1) Snowpack temperature, T_{SN}

Snowpack temperature T_{SN}, a quantity important for energy fluxes into the snow, is determined diagnostically from the state variables energy content U, and water equivalence W_{SWE}, as follows, recalling that energy content U is defined relative to 0°C ice phase.

$$T_{SN} = \frac{U}{\rho_w W_{SWE} C_i + \rho_g D_e C_g}, \qquad U < 0, \qquad \text{all solid phase} \quad \text{(S3.16)}$$

$$T_{SN} = 0, \qquad 0 < U < \rho_w W_{SWE} h_f, \qquad \text{solid and liquid mixture} \quad \text{(S3.17)}$$

$$T_{SN} = \frac{U - \rho_w W_{SWE} h_f}{\rho_w W C_w + \rho_g D_e C_g}, \qquad U > \rho_w W_{SWE} h_f, \qquad \text{all liquid phase} \quad \text{(S3.18)}$$

where $\rho_w W_{SWE} C_i$ is the heat capacity of the snow (kJ °C^{-1} m^{-2}), ρ_w is the density of water (1000 kg m^{-3}) and C_i is the specific heat of ice (2.09 kJ kg^{-1} °C^{-1}). $\rho_g D_e C_g$ is the heat capacity of the soil layer (kJ °C^{-1} m^{-2}), ρ_g is the soil density and C_g the specific heat of soil. D_e is the depth of soil that interacts thermally with the snowpack. These together determine snowpack temperature T_{SN} when energy content U<0.

Otherwise, $\rho_w W_{SWE} h_f$ is the heat required to melt all the snow water equivalence at 0 °C (kJ m^{-2}), h_f is the heat of fusion (333.5 kJ kg^{-1}) and U in relation to this determines the solid-liquid phase mixtures. The liquid fraction $L_{fr} = U/(\rho_w W_{SWE} h_f)$ quantifies the mass fraction of total snowpack (liquid and ice) that is liquid. Although in Equation S3.17 W_{SWE} is always 0 as a completely liquid snowpack cannot exist, we present this equation for completeness to keep track of energy content during periods of intermittent snow cover. $\rho_w W_{SWE} C_w$ is the heat capacity of liquid water, C_w is the specific heat of water (4.18 kJ kg^{-1} °C^{-1}), is included for numerical consistency during time steps when the snowpack completely melts.

2) Snow Surface Temperature, T_{SS}

Snow surface temperature T_{SS} is in general different from snowpack temperature T_{SN} due to the snow insulation effect. We take into account such temperature difference using an equilibrium approach that balances energy fluxes at the snow surface. Heat conduction into the snow is calculated using the temperature gradient and thermal diffusivity of snow, approximated by:

$$Q_{SN} = \frac{\kappa \rho_s C_s (T_{SS} - T_{SN})}{Z_e} = K_{SN} \rho_s C_s (T_{SS} - T_{SN}) \quad \text{(S3.19)}$$

where κ is snow thermal diffusivity ($m^2\ hr^{-1}$) and Z_e (m) an effective depth over which this thermal gradient acts. K_{SN} (κ/Z_e) is termed snow surface conductance, analogous to the heat and vapor conductance. Here K_{SN} is used as a tuning parameter, with this calculation used to define a reasonable range. Then assuming equilibrium at the surface, the surface energy balance gives:

$$Q_{SN} = Q_{sn} + Q_{li} + Q_h(T_{SS}) + Q_e(T_{SS}) + Q_p - Q_{le}(T_{SS}) \quad \text{(S3.20)}$$

where the dependence of Q_h, Q_e, and Q_{le} on T_{SS} is through equations (S3.11), (S3.12) and (S3.9) respectively. Analogous to the derivation of the Penman equation for evaporation the functions of T_{SS} in this energy balance equation are linearized about a reference temperature T^*, and the equation is solved for T_{SS}:.

$$T_{SS} = \frac{Q_{sn} + Q_{li} + Q_p + KT_a\rho_a C_p - \frac{0.622Kh_v\rho_a(e_s(T^*) - e_a - T^*\Delta)}{P_a} + 3\varepsilon_s\sigma T^{*4} + K_{SN}\rho_s C_s T_{SN}}{K_{SN}\rho_s C_s + K\rho_a C_p + \frac{0.622\Delta Kh_v\rho_a}{P_a} + 4\varepsilon_s\sigma T^{*3}} \quad \text{(S3.21)}$$

where $\Delta = de_s/dT$ and all temperatures are absolute in (K). This equation is used in an iterative procedure with an initial estimate $T^* = T_a$, in each iteration replacing T^* by the latest T_{SS}. The procedure converges to a final T_{SS} which, if less than freezing, is used to calculate surface energy fluxes. If the final T_{SS} is greater than freezing it means that the energy input to the snow surface cannot be balanced by thermal conduction into the snow. Surface melt will occur, and the infiltration of meltwater will account for the energy difference and T_{SS} is then set to 0°C.

S3.2.4 Albedo calculation

1) Ground albedo

Instead of the constant bare soil albedo in the original UEB model, the bare soil albedo is expressed as a decreasing linear function of soil moisture in STEMMUS-UEB.

$$\alpha_{g,v} = \alpha_{sat} + \min\{\alpha_{sat}, \max[(0.11 - 0.4\theta), 0]\} \quad \text{(S3.22)}$$

$$\alpha_{g,ir} = 2\alpha_{g,v} \quad \text{(S3.23)}$$

where $\alpha_{g,v}$ and $\alpha_{g,ir}$ are the bare soil/ground albedo for the visible and infrared band, respectively. α_{sat} is the saturated soil albedo, depending on local soil color. θ is the surface volumetric soil moisture.

2) Vegetation albedo

The calculation of vegetation albedo is developed to capture the essential features of a two-stream approximation model using asymptotic equation. It approaches the underlying surface albedo $\alpha_{g,\lambda}$ or the thick canopy albedo $\alpha_{c,\lambda}$ when the L_{SAI} is close to zero or infinity.

$$\alpha_{Veg,b,\lambda} = \alpha_{c,\lambda}\left[1 - \exp\left(-\frac{\omega_\lambda \beta L_{SAI}}{\mu \alpha_{c,\lambda}}\right)\right] + \alpha_{g,\lambda}\exp[-\left(1 + \frac{0.5}{\mu}\right)L_{SAI}] \quad \text{(S3.24)}$$

$$\alpha_{Veg,d,\lambda} = \alpha_{c,\lambda}\left[1 - \exp\left(-\frac{2\omega_\lambda \beta L_{SAI}}{\alpha_{c,\lambda}}\right)\right] + \alpha_{g,\lambda}\exp[-2\,L_{SAI}] \quad \text{(S3.25)}$$

where subscripts Veg, b, d, c, g and λ represent vegetation, direct beam, diffuse radiation, thick canopy, ground, and spectrum bands of either visible or infrared bands. μ is the cosine of solar zenith angle; ω_λ is the single scattering albedo, 0.15 for visible and 0.85 for infrared band, respectively; β is assigned as 0.5; L_{SAI} is the sum of leaf area index LAI and stem area index SAI; $\alpha_{c,\lambda}$ is the thick canopy albedo dependent on vegetation types.

The bulk snow-free surface albedo, averaged between bare ground albedo and vegetation albedo, then is written as:

$$\alpha_{\eta,\lambda} = \alpha_{Veg,\lambda} f_{Veg} + \alpha_{g,\lambda}(1 - f_{Veg}) \quad \text{(S3.26)}$$

where $\alpha_{\eta,\lambda}$ is the averaged bulk snow-free surface albedo; f_{Veg} is the fraction of vegetation cover.

3) Snow albedo

According to Dickinson et al. (1993), snow albedo can be expressed as a function of snow surface age and solar illumination angle. The snow surface age, which is dependent on snow surface temperature and snowfall, is updated with each time step in UEB. Visible and near infrared bands are separately treated when calculating reflectance, which are further averaged as the albedo with modifications of illumination angle and snow age. The reflectance in the visible and near infrared bands can be written as:

$$\alpha_{vd} = \left(1 - C_v S_{age}\right)\alpha_{vo} \quad \text{(S3.27)}$$

$$\alpha_{ird} = \left(1 - C_{ir} S_{age}\right)\alpha_{iro} \quad \text{(S3.28)}$$

where α_{vd} and α_{ird} represent diffuse reflectance in the visible and near infrared bands, respectively. C_v (= 0.2) and C_{ir} (=0.5) are parameters that quantify the sensitivity of the visible and infrared band albedo to snow surface aging (grain size growth), α_{vo} (=0.85) and α_{iro} (=0.65) are fresh snow reflectance in visible and infrared bands, respectively. S_{age} is a function to account for aging of the snow surface, and is given by

$$S_{age} = \frac{\tau}{1 + \tau} \quad \text{(S3.29)}$$

where τ is the non-dimensional snow surface age that is incremented at each time step by the quantity designed to emulate the effect of the growth of surface grain sizes.

$$\Delta\tau = \frac{r_1 + r_2 + r_3}{\tau_o}\Delta t \quad \text{(S3.30)}$$

where Δt is the time step in seconds with $\tau_o = 10^6$s. r_1 is the parameter to represent the effect of grain growth due to vapor diffusion, and is dependent on snow surface temperature:

$$r_1 = \exp\left[5000\left(\frac{1}{273.16} - \frac{1}{T_s}\right)\right] \quad \text{(S3.31)}$$

r_2 describes the additional effect near and at the freezing point due to melt and refreeze:

$$r_2 = \min\left(r_1^{10}, 1\right) \quad \text{(S3.32)}$$

r_3=0.03 (0.01 in Antarctica) represents the effect of dirt and soot.

The reflectance of radiation with illumination angle (measured relative to the surface normal) is computed as:

$$\alpha_v = \alpha_{vd} + 0.4\, f(\varphi)(1 - \alpha_{vd}) \quad \text{(S3.33)}$$

$$\alpha_{ir} = \alpha_{ird} + 0.4\, f(\varphi)(1 - \alpha_{ird}) \quad \text{(S3.34)}$$

where $f(\varphi) = \begin{cases} \frac{1}{b}\left[\frac{b+1}{1+2b\cos(\varphi)} - 1\right], & for\ \cos(\varphi) < 0.5 \\ 0, & otherwise \end{cases}$

where b is a parameter set at 2 as Dickinson et al. (1993).

When the snowpack is shallow (depth z<h=0.01m), the albedo is calculated by interpolating between the snow albedo and bare ground albedo with the exponential term approximating the exponential extinction of radiation penetration of snow.

$$A_{v/ir} = r\alpha_{g,v/ir} + (1 - r)\alpha_{v/ir} \quad \text{(S3.35)}$$

where $r = \left(1 - \frac{z}{h}\right) e^{-z/2h}$.

S4 STEMMUS-UEB: Coupling structure, Subroutines and Input Data

S4.1 Coupling procedure

The coupled process between the snowpack model (UEB) and the soil water model (STEMMUS-FT) is illustrated in Figure S4.1. The sequential coupling is employed to couple the soil model with the current snowpack model. The role of the snowpack is explicitly considered by altering the water and heat flow of the underlying soil. The snowpack model takes the atmospheric forcing as the input (precipitation, air temperature, wind speed and direction, relative humidity, shortwave and longwave radiation) and solves the snowpack energy and mass balance (Eqs. S3.1 & S3.2, Subroutines: ALBEDO, PARTSNOW, PREDICORR), provides the melt water flux and heat flux as the surface boundary conditions for the soil model STEMMUS-FT (Subroutines: h_sub and Enrgy_sub for ACD models; Diff_Moisture_Heat for BCD model). The soil-snow coupling variables are the snowmelt water flux M_r, the convective heat flux due to snowmelt water Q_m and the heat conduction flux Q_g. STEMMUS-FT then solves the energy and mass balance equations of soil layers in one timestep. To highlight the effect of snowpack on the soil water and

vapor transfer process, we constrained the soil surface energy boundary as the Dirichlet type condition (take the specific soil temperature as the surface boundary condition). Surface soil temperature was derived from the soil profile measurements and not permitted to be higher than zero when there is snowpack. In such way, the reliability of the soil surface energy boundary condition is maintained, and the snow thermal effect is implicitly considered. The snowmelt water flux, in addition to the rainfall, was added to the topsoil boundary for solving soil water transfer. To ensure the numerical convergence, the adapted timestep strategy was used. The half-hourly meteorological forcing measurements were linearly interpolated to the running timesteps (Subroutine Forcing_PARM). The precipitation rate (validated at 3-hour time intervals) was regarded uniformly within the 3-hour duration (see Table S6.1 for detail). The general description of the subroutines in STEMMUS-UEB, including the main functions, input/output, and its connection with other subroutines, was presented in Table S4.1 & S4.2 (linked with Table S6.1 and S6.2 for the description of model input parameters and outputs for this study).

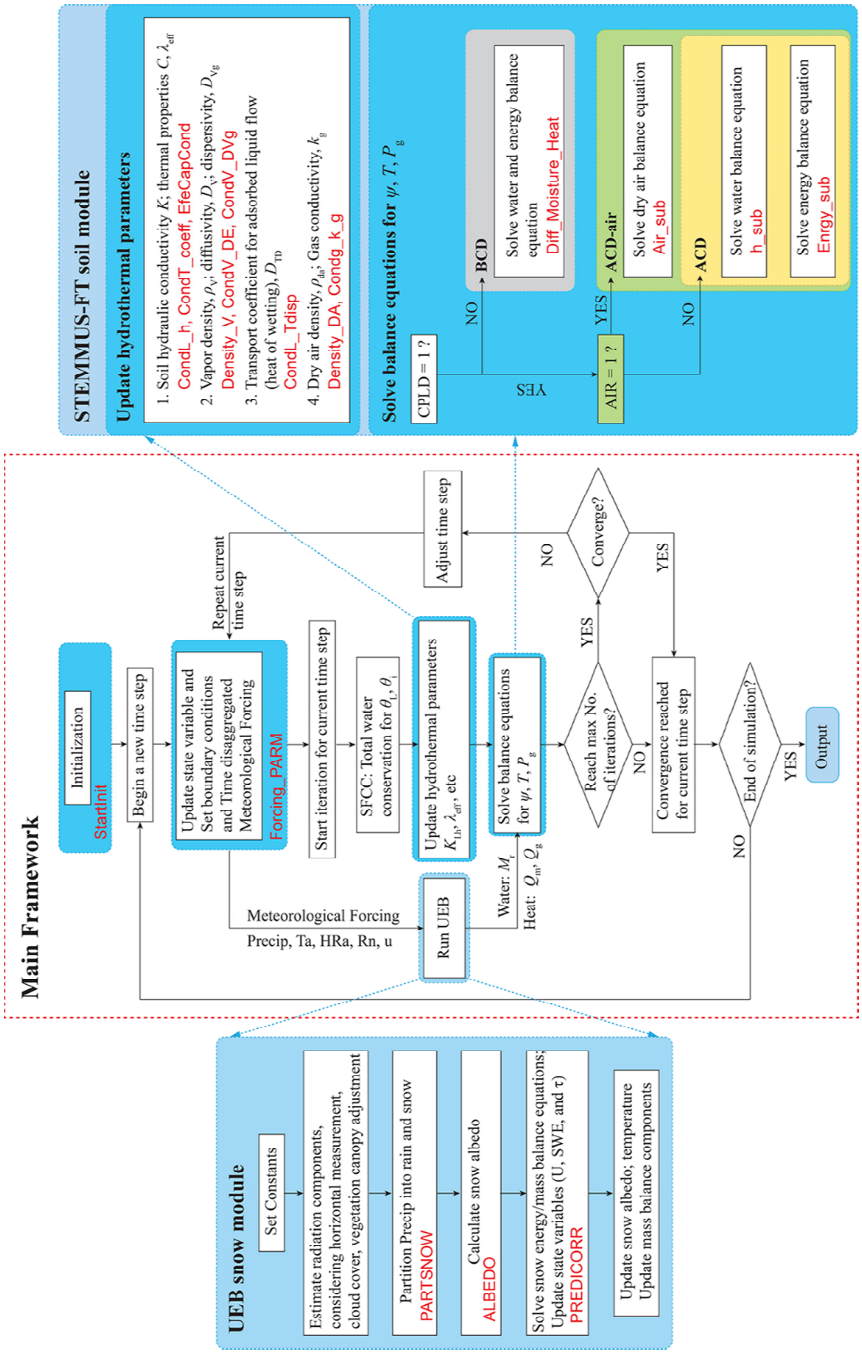

Figure S4.1. The overview of the coupled STEMMUS-FT and UEB model framework and model structure. SFCC is soil freezing characteristic curve; θ_L and θ_i are soil liquid water and ice content; K_{Lh} is soil hydraulic conductivity; λ_{eff} is thermal conductivity. ψ, T, P_g are the state variables for soil module STEMMUS-FT (matric potential, temperature, and air pressure, respectively). U, SWE, and τ are the state variables for snow module UEB (snow energy content, snow water equivalent, and snow age, respectively). UEB, Utah Energy Balance module. Precip, Ta, HRa, Rn, and u are the meteorological inputs (precipitation, air temperature, relative humidity, radiation and wind speed). M_r is the snowmelt water flux, Q_m is the convective heat flux due to snowmelt water and Q_g is the heat conduction flux. Model subroutines are in red fonts.

S4.2 Subroutines and Inputs/Outputs

Table S4.1 and Table S4.2 summarize the main functions, input/output, and code inter-connections of the primary subroutines and secondary subroutines, which presents the complete Input-Primary Subroutine-Secondary Subroutine-Output loop of STEMMUS-UEB modelling framework.

565 STEMMUS-UEB model subroutines can be generally divided into four groups as identified by different calling sequential orders or roles/functions in the main program: Initialization Group, Parameterization Group, Processing Group, and Post-process Group. Note that some subroutines can be categorized into more than one group, we made the classification based on the functions of the subroutine here. For example, subroutine SOIL2 is called by subroutine StartInit, which belongs to the Initialization Group. Nevertheless, 570 according to the function of SOIL2, it falls into the Parameterization Group. We then label SOIL2 as Parameterization Group.

Table S4.1. Primary subroutines in STEMMUS-UEB

Model Subroutines	Main functions	Main inputs	Main outputs	Subroutine-Connections	Remarks
Soil module					
Air_sub	Solves soil dry air balance equation	Water vapor density, diffusivity, dispersion coefficient, dry air density, gas conductivity, flux, liquid water flux, top and bottom boundary conditions	Soil air pressure profile	CondV_DVg, CondL_h, Condg_k_g, Density_V, h_sub --->; --> Enrgy_sub,	Processing Group
CondL_h	Calculates soil hydraulic conductivity	Soil hydraulic parameters, soil matric potential, soil temperature	Soil hydraulic conductivity, soil water content	StartInit --->; --> h_sub, Air_sub, Enrgy_sub,	Parameterization Group
CondT_coeff	Calculates soil thermal capacity and conductivity	Thermal properties of soil constituents, soil texture, soil water content, volumetric fraction of dry air, dry air density, vapor density	Soil thermal capacity and conductivity	StartInit, CondL_h, Density_V, Density_DA, EfeCapCond --->; --> Enrgy_sub,	Parameterization Group
CondV_DVg	Calculates flux of dry air and vapor dispersity	Gas conductivity, dry air pressure, volumetric fraction of dry air, saturated soil water content	Dry air flux and vapor dispersion coefficient	StartInit, CondL_h, Condg_k_g --->; --> h_sub, Air_sub, Enrgy_sub,	Parameterization Group
CondL_Tdisp	Calculates transport coefficient for adsorbed liquid flow	Soil porosity, soil water content, temperature, matric potential, volumetric fraction of dry air	Transport coefficient for adsorbed liquid flow and the heat of wetting	StartInit, CondL_h, Condg_k_g --->; --> h_sub, Enrgy_sub,	Parameterization Group
Condg_k_g	Calculates gas conductivity	Soil porosity, saturated hydraulic conductivity, volumetric fraction of dry air	Gas conductivity	StartInit, CondL_h --->; --> CondV_DVg,	Parameterization Group
Density_DA	Calculates dry air density	Soil temperature, matric potential, dry air pressure, vapor density and its derivative with respect to temperature and matric potential	Density of dry air	StartInit, CondL_h, Density_V --->; --> CondT_coeff, Air_sub, Enrgy_sub,	Parameterization Group
Density_V	Calculates vapor density and its derivative with respect to temperature and matric potential	Soil temperature, matric potential	Vapor density and its derivative with respect to temperature and matric potential	CondL_h --->; --> Density_DA, CondT_coeff, h_sub, Air_sub, Enrgy_sub,	Parameterization Group
EfeCapCond	Calculates soil thermal	Thermal properties of soil constituents, soil texture, soil	Soil heat capacity, thermal	StartInit, CondL_h, Density_V, Density_DA -	Parameterization Group

	capacity and conductivity	water content, volumetric fraction of dry air, dry air density, vapor density	conductivity	-->; --> CondT_coeff,	
Enrgy_sub	Solves soil energy balance equation	Soil thermal properties, soil hydraulic conductivity, soil matric potential, soil water content, soil temperature, soil dry air pressure, density of dry air, heat of wetting, vapor density, liquid water flux, vapor flux, dry air flux, meterological forcing, top and bottom boundary conditions	Soil temperature profile, liquid water flux, vapor flux, and dry air flux, surface and bottom energy fluxes	Air_sub, h_sub, CondL_h, CondV_DVg, CondL_Tdisp, CondT_coeff, Density_D, Density_DA, PREDICORR --->,	Processing Group
Forcing_PARM	Disaggregates the meteorological forcing into the required time steps	Observed meteorological forcing at hourly/daily time scale	Meteorological forcings at model required time scale	StartInit --->; --> h_sub, Enrgy_sub,	Initialization Group
h_sub	Solves soil water balance equation	Soil temperature, soil water content, matric potential, soil hydraulic conductivity, heat of wetting, soil dry air pressure, vapor density, diffusivity, dispersity, volumetric fraction of vapor, meteorological forcing, top and bottom boundary conditions	Soil matric potential profile, top and bottom water fluxes, evaporation	StartInit, CondV_DVg, CondL_h, CondV_DE, CondL_Tdisp, Condg_k_g, Density_V, Forcing_PARM, ALBEDO, PARTSNOW, PREDICORR --->; --> Air_sub, Enrgy_sub,	Processing Group
StartInit	Initializes model setup	Soil texture, thermal properties of soil constituents, initial soil water content and temperature, top and bottom boundary condition settings	-	--> CondV_DVg, CondL_h, CondV_DE, CondL_Tdisp, Condg_k_g, Density_DA, EfeCapCond, Forcing_PARM, h_sub,	Initialization Group
Diff_Moisture_Heat	Solves soil water and energy balance equations independently	Soil thermal properties, soil hydraulic conductivity, soil matric potential, soil water content, soil temperature, meteorological forcing, top and bottom boundary conditions	Soil water content and temperature profile, liquid water flux, surface and bottom water and energy fluxes	StartInit, CondT_coeff, Forcing_PARM, ALBEDO, PARTSNOW, PREDICORR --->,	Processing Group
Snowpack module					
agesn	Calculates snow age	Snow surface temperature, snowfall	Updated snow age	PARTSNOW, PREDICORR --->; --> ALBEDO,	Parameterization Group
ALBEDO	Calculates snow albedo	Fresh snow reflectance at visible and near infrared bands, snow age, bare ground albedo, albedo extinction parameter, snow water equivalent	Snow albedo	agesn --->; --> PREDICORR,	Parameterization Group
PARTSNOW	Partitions precipitation into rainfall and snowfall	Precipitation, air temperature, temperature thresholds for rainfall/snowfall	Rainfall, snowfall	Forcing_PARM --->; --> PREDICORR,	Parameterization Group
PREDICORR	Solves the snow mass and energy balance equations and updates state variables SWE and U	Air temperature, snow albedo, wind speed, relative humidity, rainfall/snowfall, shortwave/longwave radiation, site parameters	Snow energy content, water equivalent, snow albedo, snow surface temperature, meltwater outflow rate, snow sublimation, snowfall/rainfall	Forcing_PARM --->; --> agesn^2, ALBEDO^2.	Processing Group

Note:

---> means the relevant subroutines which are incoming to the current one, --> means the relevant subroutines for which the current subroutine is output to;

agesn^2 and ALBEDO^2, means the use of subroutines agesn and ALBEDO after solving the snowpack energy and mass conservation equations, to update the snow age and albedo.

Table S4.2. Secondary subroutines in STEMMUS-UEB

Model Subroutines	Main functions	Main inputs	Main outputs	Subroutine-Connections	Remarks
Soil module					
Constants	Set the constants	Water vapor density, diffusivity, dispersion coefficient, dry air density, gas conductivity, flux, liquid water flux, top and bottom boundary conditions	Soil air pressure profile	Initializing the following subroutines	Initialization Group
Dtrmn_Z	User define the vertical discretization Δz	Soil column depth, layer number	Thickness of each soil layer	--> Constants	Initialization Group
SOIL2	Calculate soil moisture θ_L	Soil hydraulic parameters, soil matric potential, soil temperature	Soil hydraulic conductivity, soil water content	--> StartInit, MainLoop	Parameterization Group
Latent	Calculate the latent heat L	Soil temperature	Latent heat	--> Diff_Moisture_Heat, MainLoop	Parameterization Group
Evap_Cal	Calculate albedo, evaporation, and root water uptake	Soil moisture, temperature, meteorological forcing, time	Soil evaporation, resistance, albedo, root water uptake, transpiration	--> h_BC	Parameterization Group
SOIL1	Update the wetting history	Soil moisture at previous and current time step, indicator of the wetting/drying status	Updated indicator of the wetting/drying status	--> MainLoop	Processing Group
hPARM	Calculate the matrices coefficient for liquid equation	Soil temperature, soil water content, matric potential, soil hydraulic conductivity, vapor density, diffusivity, dispersity, volumetric fraction of vapor	Matrices coefficient for liquid equation	StartInit, CondV_DVg, CondL_h, CondV_DE, CondL_Tdisp, Condg_k_g, Density_V, Forcing_PARM--->; --> h_MAT, h_sub,	Processing Group
h_MAT	Assemble the global coefficient matrices of the Galerkin expressions for liquid equation	Matrices coefficient for liquid equation	Global coefficient matrices for liquid equation	hPARM --->; --> h_EQ, h_sub,	Processing Group
h_EQ	Perform the finite difference of the time derivatives in the matrix equation	Global coefficient matrices for liquid equation	Updated right-hand side values	h_MAT --->; --> h_Solve, h_sub,	Processing Group
h_BC	Set the boundary condition for solving liquid equation	Soil temperature, soil water content, matric potential, soil hydraulic conductivity, meteorological forcing, top and bottom boundary conditions	Global coefficient matrices at boundary nodes	StartInit, Evap_Cal, h_MAT, ALBEDO, PARTSNOW, PREDICORR --->; --> h_Solve, h_sub,	Processing Group
h_Solve	Solve the matrix equation for liquid conservation	Global coefficient matrices of all nodes	Updated soil matric potential profile	h_EQ, h_BC --->; --> h_Bndry_Flux, h_sub,	Processing Group
h_Bndry_Flux	Calculate liquid flux of the boundary node	Updated soil matric potential profile	Top and bottom water fluxes	h_Solve --->; --> h_sub,	Processing Group
AirPARM	Calculate the matrices coefficient for dry air equation	Dry air pressure, density, gas conductivity, flux, water vapor density, diffusivity, dispersion coefficient, soil matric potential, water content, temperature, conductivity	Matrices coefficient for dry air equation	CondV_DVg, CondL_h, Condg_k_g, Density_V, h_sub --->; --> Air_MAT, Air_sub,	Processing Group
Air_MAT	Assemble the global coefficient matrices of the Galerkin expressions for dry air equation	Matrices coefficient for dry air equation	Global coefficient matrices for dry air equation	AirPARM --->; --> Air_EQ, Air_sub,	Processing Group

Air_EQ	Perform the finite difference of the time derivatives in the matrix equation for dry air	Global coefficient matrices for dry air equation	Updated right-hand side values	Air_MAT, h_sub --->; --> Air_Solve, Air_sub,	Processing Group
Air_BC	Set the boundary condition for solving dry air equation	Top and bottom boundary conditions	Global coefficient matrices at boundary nodes	StartInit, Air_MAT --->; --> Air_Solve, Air_sub,	Processing Group
Air_Solve	Solve the matrix equation for dry air conservation	Global coefficient matrices of all nodes	Soil air pressure profile	Air_BC, Air_EQ --->; --> Air_sub,	Processing Group
EnrgyPARM	Calculate the matrices coefficient for energy equation	Soil temperature, soil water content, matric potential, soil hydraulic conductivity, vapor density, diffusivity, dispersity, volumetric fraction of vapor, soil thermal properties, soil dry air pressure, conductivity, air flux	Matrices coefficient for energy equation, liquid, vapor, and dry air flux	Air_sub, h_sub, CondL_h, CondV_DVg, CondL_Tdisp, CondT_coeff, Density_D, Density_DA, PREDICORR --->, --> Enrgy_MAT, Enrgy_sub	Processing Group
Enrgy_MAT	Assemble the global coefficient matrices of the Galerkin expressions for energy equation	Matrices coefficient for energy equation	Global coefficient matrices for energy equation	EnrgyPARM --->, --> Enrgy_EQ, Enrgy_sub	Processing Group
Enrgy_EQ	Perform the finite difference of the time derivatives in the matrix equation for energy	Global coefficient matrices for energy equation	Updated right-hand side values	Air_sub, h_sub, Enrgy_MAT --->, --> Enrgy_Solve, Enrgy_sub	Processing Group
Enrgy_BC	Set the boundary condition for solving energy equation	Top and bottom boundary conditions	Global coefficient matrices at boundary nodes	StartInit, Enrgy_MAT --->, --> Enrgy_Solve, Enrgy_sub	Processing Group
Enrgy_Solve	Solve the matrix equation for energy conservation	Global coefficient matrices of all nodes	Soil temperature profile	Enrgy_EQ, Enrgy_BC --->, --> Enrgy_Bndry_Flux, Enrgy_sub	Processing Group
Enrgy_Bndry_Flux	Calculate energy flux of the boundary node	Soil temperature profile	Surface and bottom energy fluxes	Enrgy_Solve --->, --> Enrgy_sub	Processing Group
TimestepCHK	Assessing the change in boundary conditions after one time step	Surface boundary conditions, time step, indicators of the boundary condition change	Updated time step and indicators of the boundary condition change	h_sub, Air_sub, Enrgy_sub, SOIL2 --->,	Post-processing Group
CnvrgnCHK	Check the convergence	Soil state variables, convergence criteria, time step, indicators of the boundary condition change	Updated time step and indicators of the boundary condition change	h_sub, Enrgy_sub, SOIL2 --->, --> TimestepCHK	Post-processing Group
PlotResults	Plot the results				Post-processing Group
Snowpack module					
atf	Calculate the atmospheric transmissivity	Date, Campbell coefficient	Atmospheric transmissivity	--> snow_Calc	Parameterization Group
Cosen	Calculate the hourly radiation index	Date, slope, latitude	Hourly radiation index	--> Eavp_Cal	Parameterization Group
hyri	Calculate the hourly radiation index	Date, slope, latitude	Hourly radiation index	--> snow_Calc	Parameterization Group
FMELT	Calculate the melt rate and outflow	Energy content, snow water equivalent, snow saturated hydraulic conductivity, precipitation	Melt outflow rate	--> QFM	Parameterization Group
JULIAN	Convert the real date to julian date	Date (mm, dd)	Julian date (001-365/366)	--> hyri	Parameterization Group

PREHELP	Correct energy and mass fluxes when numerical overshoots	Rainfall/snowfall, snow equivalent, snow energy components	Corrected snow mass and energy fluxes	QFM --->, --> PREDICORR	Processing Group
QFM	Calculate snow mass and energy fluxes	Snow water equivalent, energy content, rainfall/snowfall, meteorological forcing, site information	Snow mass and energy fluxes	FMELT, QPF, SVPW, TAVG, TURBFLUX, SRFTMP --->, --> PREDICORR	Parameterization Group
qlif	Compute the incoming longwave radiation	Air temperature, relative humidity, cloud fraction	Incoming longwave radiation	--> snow_Calc	Parameterization Group
QPF	Calculate the heat advected to the snowpack	Precipitation, air temperature	Snow heat advection due to rain	--> QFM	Parameterization Group
RKINST	Calculate no neutral turbulent transfer coefficient	Wind speed, air temperature, surface temperature	Turbulent transfer coefficient	--> TURBFLUX	Parameterization Group
SRFTMP	Compute snow surface temperature	Surface energy components, meteorological forcing	Snow surface temperature	surfeb --->, --> QFM	Parameterization Group
surfeb	Solve the surface energy balance for surface temperature	Surface energy components, meteorological forcing	Updating surface energy balance	--> SRFTMP	Parameterization Group
SVP	Calculate the vapor pressure over water or ice	Temperature	Vapor pressure	--> surfeb	Parameterization Group
SVPI	Calculate the vapor pressure over ice	Temperature	Vapor pressure over ice	--> TURBFLUX	Parameterization Group
SVPW	Calculate the vapor pressure over water	Temperature	Vapor pressure over water	--> QFM, qlif	Parameterization Group
TAVG	Calculate the average temperature of snow and the interacting soil layer	Snow water and energy content, soil and snow heat properties	Average temperature of snow and the interacting soil layer	--> QFM, snow_Calc	Parameterization Group
TURBFLUX	Calculate the turbulent heat fluxes	Precipitation, surface temperature, vapor pressure, wind speed, turbulent transfer coefficient	Turbulent heat fluxes and condensation/sublimation	RKINST, SVPI --->, --> QFM	Parameterization Group
UPDATETIME	Update time for each time step	Date (yy, mm, dd, hh)	Updated time	--> snow_Calc	Parameterization Group

Note:

---> means the relevant subroutines which are incoming to the current one, --> means the relevant subroutines for which the current subroutine is output to.

S4.3 Setup and Running the model

The current STEMMUS-UEB is tested with MATLAB 2019b. STEMMUS-UEB is executed in MATLAB by simply running MainLoop.m after you finish all the model setup and give the input data to STEMMUS-UEB. Several steps are necessary to build up the model setup.

1. Setting the temporal information and model domain.
2. Setting soil properties and snow properties.
3. Setting the initialization condition for soil and snow submodules, respectively.
4. Inputting the meteorological forcing information.
5. Setting the surface/bottom conditions.

Then you are ready to run STEMMUS-UEB by running MainLoop.m.

S4.4 List of model variables

Table S4.3 summarizes the main model parameters/variables and divides them into input and output parameters/variables. Some of the value for the input parameters are also listed.

Table S4.3. The descriptions of the main model input/output variables

Symbol	Parameter	Unit	Value
Main inputs			
Soil model component (STEMMUS-FT)			
a	Fitted parameter for soil surface resistance	-	0.3565
$b(z)$	Normalized water uptake distribution	m^{-1}	
C_a	Specific heat capacity of dry air	J kg^{-1} $°C^{-1}$	1.005
C_{app}	Apparent heat capacity	J kg^{-1} $°C^{-1}$	
C_i	Specific heat capacity of ice	J kg^{-1} $°C^{-1}$	2.0455
C_L	Specific heat capacity of liquid	J kg^{-1} $°C^{-1}$	4.186
C_s	Specific heat capacity of soil solids	J kg^{-1} $°C^{-1}$	
C_{soil}	Heat capacity of the bulk soil	J kg^{-1} $°C^{-1}$	
C_V	Specific heat capacity of water vapor	J kg^{-1} $°C^{-1}$	1.87
c_p	Specific heat capacity of air	J kg^{-1} K^{-1}	
D_e	Molecular diffusivity of water vapor in soil	m^2 s^{-1}	
D_{TD}	Transport coefficient for adsorbed liquid flow due to temperature gradient	kg m^{-1} s^{-1} $°C^{-1}$	
D_{Va}	Advective vapor transfer coefficient	s	
D_{Vg}	Gas phase longitudinal dispersion coefficient	m^2 s^{-1}	
D_{Vh}	Isothermal vapor conductivity	kg m^{-2} s^{-1}	
D_{VT}	Thermal vapor diffusion coefficient	kg m^{-1} s^{-1} $°C^{-1}$	
H_c	Henry's constant	-	0.02
K	Hydraulic conductivity	m s^{-1}	
K_g	Intrinsic air permeability	m^2	
K_{Lh}	Isothermal hydraulic conductivities	m s^{-1}	
K_{LT}	Thermal hydraulic conductivities	m^2 s^{-1} $°C^{-1}$	
K_s	Soil saturated hydraulic conductivity	m s^{-1}	
L_0	Latent heat of vaporization of water at the reference temperature	J kg^{-1}	
LAI_{eff}	Effective leaf area index	-	
L_f	Latent heat of fusion	J kg^{-1}	3.34E+05
n	Van Genuchten fitting parameters	-	
r_a^c	Aerodynamic resistance for canopy surface	s m^{-1}	
r_a^s	Aerodynamic resistance for bare soil	s m^{-1}	
$r_{c,min}$	Minimum canopy surface resistance	s m^{-1}	
$r_{l,min}$	Minimum leaf stomatal resistance	s m^{-1}	
r_s	Soil surface resistance	s m^{-1}	
r_{sl}	Resistance to molecular diffusion of the water surface	s m^{-1}	10
R_n	Net radiation	MJ m^{-2} day^{-1}	
R_n^c	Net radiation at the canopy surface	MJ m^{-2} day^{-1}	
R_n^s	Net radiation at the soil surface	MJ m^{-2} day^{-1}	

S_a	Degree of saturation of the soil air	-	$=1-S_L$
S_L	Degree of water saturation in the soil	-	$=\theta_L/\varepsilon$
S_p	Potential water uptake rate	s^{-1}	
t	Time	s	
T_p	Potential transpiration	m s^{-1}	
T_r	Arbitrary reference temperature	°C	20
W	Differential heat of wetting	J kg^{-1}	
z	Vertical space coordinate (positive upwards)	m	
α	Air entry value of soil	m^{-1}	
$a(h)$	Reduction coefficient related to soil water potential	-	
ε	Porosity	-	
λ_{eff}	Effective thermal conductivity of the soil	W m^{-1} °C^{-1}	
θ_s	Volumetric fraction of solids in the soil	m^3 m^{-3}	
θ_{sat}	Saturated soil water content	m^3 m^{-3}	
θ_r	Residual soil water content	m^3 m^{-3}	
θ_1	Topsoil water content	m^3 m^{-3}	
θ_{min}	Minimum water content above which soil is able to deliver vapor at a potential rate	m^3 m^{-3}	
ρ_a	Air density	kg m^{-3}	
ρ_{da}	Density of dry air	kg m^{-3}	
ρ_i	Density of ice	kg m^{-3}	920
ρ_L	Density of soil liquid water	kg m^{-3}	1000
ρ_s	Density of solids	kg m^{-3}	
ρ_V	Density of water vapor	kg m^{-3}	
γ_W	Specific weight of water	kg m^{-2} s^{-2}	
μ_a	Air viscosity	kg m^{-2} s^{-1}	
Snow model component (UEB)			
T_r	Air temperature above which precipitation is all rain	°C	
T_{sn}	Air temperature below which precipitation is all snow	°C	
ε_{sn}	Emissivity of snow	-	
C_g	Ground heat capacity	J kg^{-1} °C^{-1}	
z_o	Snow surface aerodynamic roughness	m	
L_c	Liquid holding capacity of snow	-	
K_{sn}	Snow saturated hydraulic conductivity	m h^{-1}	
α_{vo}	Visual new snow albedo	-	
α_{iro}	Near-infrared new snow albedo	-	
α_{bg}	Bare ground albedo	-	Eqs. S3.22-S3.26
D_e	Thermally active depth of soil	m	
λ_{sn}	Snow surface thermal conductivity	m h^{-1}	
ρ_{sn}	Snow density	kg m^{-3}	
A_{ed}	Albedo extinction depth	m	
F_c	Forest cover fraction	-	
D_f	Drift factor	-	
ρ_s	Soil density	kg m^{-3}	

Main outputs		
Soil model component (STEMMUS-FT)		
ψ	Soil water potential	m
P_g	Mixed pore-air pressure	Pa
T	Soil temperature	°C
θ	Volumetric water content	$m^3\ m^{-3}$
θ_i	Soil ice volumetric water content	$m^3\ m^{-3}$
θ_L	Soil liquid volumetric water content	$m^3\ m^{-3}$
θ_V	Soil vapor volumetric water content	$m^3\ m^{-3}$
θ_a	Volumetric fraction of dry air in the soil	$m^3\ m^{-3}$
q	Water flux	$kg\ m^{-2}\ s^{-1}$
q_a	Dry air flux	$kg\ m^{-2}\ s^{-1}$
q_L	Soil liquid water fluxes (positive upwards)	$kg\ m^{-2}\ s^{-1}$
q_{La}	Liquid water flux driven by the gradient of air pressure	$kg\ m^{-2}\ s^{-1}$
q_{Lh}	Liquid water flux driven by the gradient of matric potential	$kg\ m^{-2}\ s^{-1}$
q_{LT}	Liquid water flux driven by the gradient of temperature	$kg\ m^{-2}\ s^{-1}$
q_V	Soil water vapor fluxes (positive upwards)	$kg\ m^{-2}\ s^{-1}$
q_{Va}	Water vapor flux driven by the gradient of air pressure	$kg\ m^{-2}\ s^{-1}$
q_{Vh}	Water vapor flux driven by the gradient of matric potential	$kg\ m^{-2}\ s^{-1}$
q_{VT}	Water vapor flux driven by the gradient of temperature	$kg\ m^{-2}\ s^{-1}$
S	Sink term for transpiration	s^{-1}
S_h	Latent heat flux density	$W\ m^{-3}$
Snow model component (UEB)		
P_r	Precipitation in the form of rain	$m\ s^{-1}$
P_s	Precipitation in the form of snow	$m\ s^{-1}$
W_{SWE}	Snow water equivalent	m
Q_h	Surface Sensible Heat Flux	$W\ m^{-2}$
Q_e	Surface Latent Heat Flux	$W\ m^{-2}$
E	Surface Sublimation	$m\ s^{-1}$
T_{SS}	Snow Surface Temperature	°C
U	Energy Content	
M_r	Melt outflow rate	$m\ s^{-1}$
$A_{v/ir}$	Surface Albedo	-
Q_m	Heat advected by melt outflow	$W\ m^{-2}$
Q_{sn}	Net shortwave radiation	$W\ m^{-2}$
Q_{li}	Net longwave radiation	$W\ m^{-2}$
τ	No-dimensional snow age	-

600

S5 Additional results: Understanding the water/heat transfer mechanisms in frozen soil

This section presents the example modelling results, illustrating the model capability in terms of detailed interpretation of water/heat transfer mechanisms. The analysis of water fluxes is shown in Section S5.1 (see Yu et al., 2018 for detail). Section S5.2 conducted the heat budget analysis (see Yu et al., 2020b for detail).

S5.1 Water flux analysis

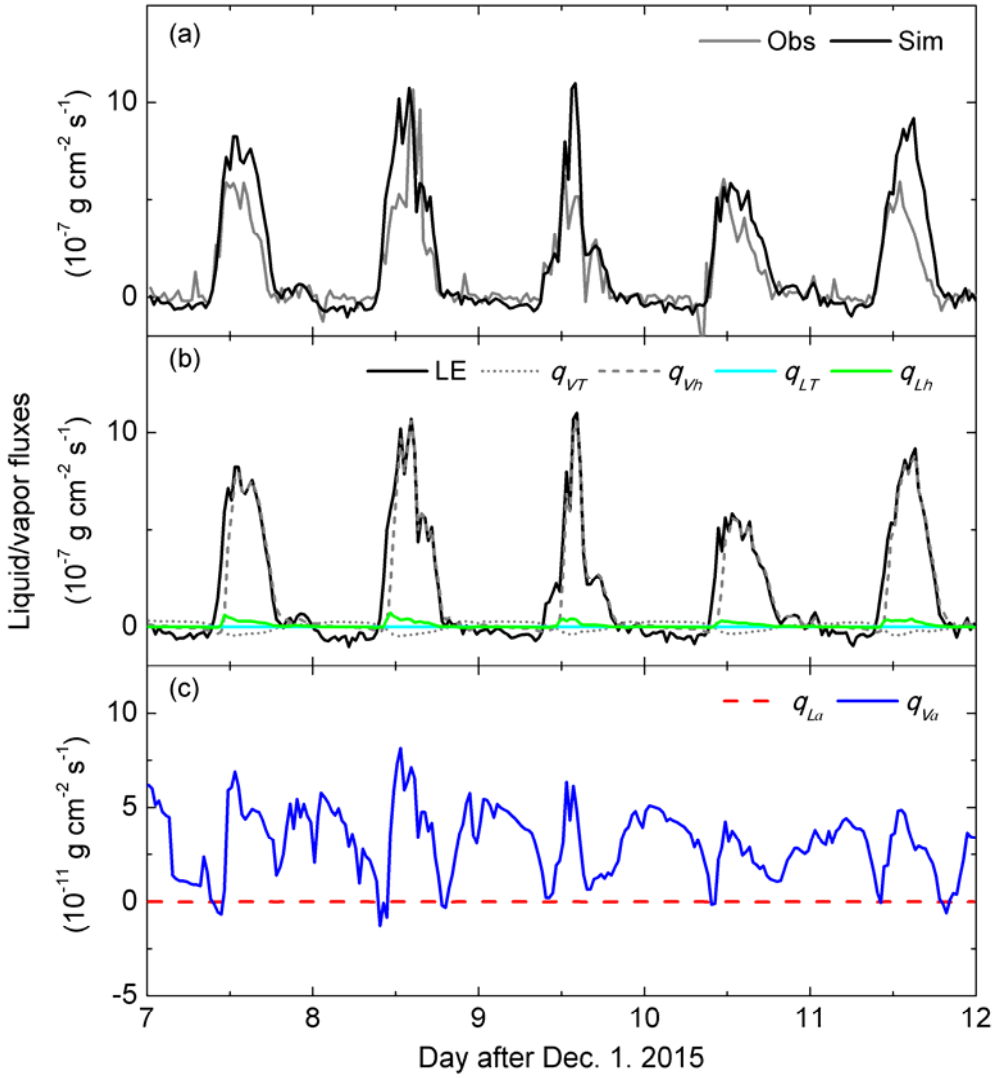

Figure S5.1. Observed latent heat flux and simulated (a) latent heat flux and (b) surface soil (0.1cm) thermal and isothermal liquid water and vapor fluxes (LE, q_{VT}, q_{Vh}, q_{LT}, q_{Lh}) (c) surface soil (0.1cm) advective liquid water and vapor fluxes (q_{La}, q_{Va}) of a typical five-day freezing period (from 8th to 12th Days after Dec. 1. 2015). LE is the latent heat flux, q_{VT}, q_{Vh} are the water vapor fluxes driven by temperature and matric potential gradients, q_{LT}, q_{Lh} are the liquid water fluxes driven by temperature and matric potential gradients, q_{La}, q_{Va} are the liquid and vapor water fluxes driven by air pressure gradients. Positive/negative values indicate upward/downward fluxes.

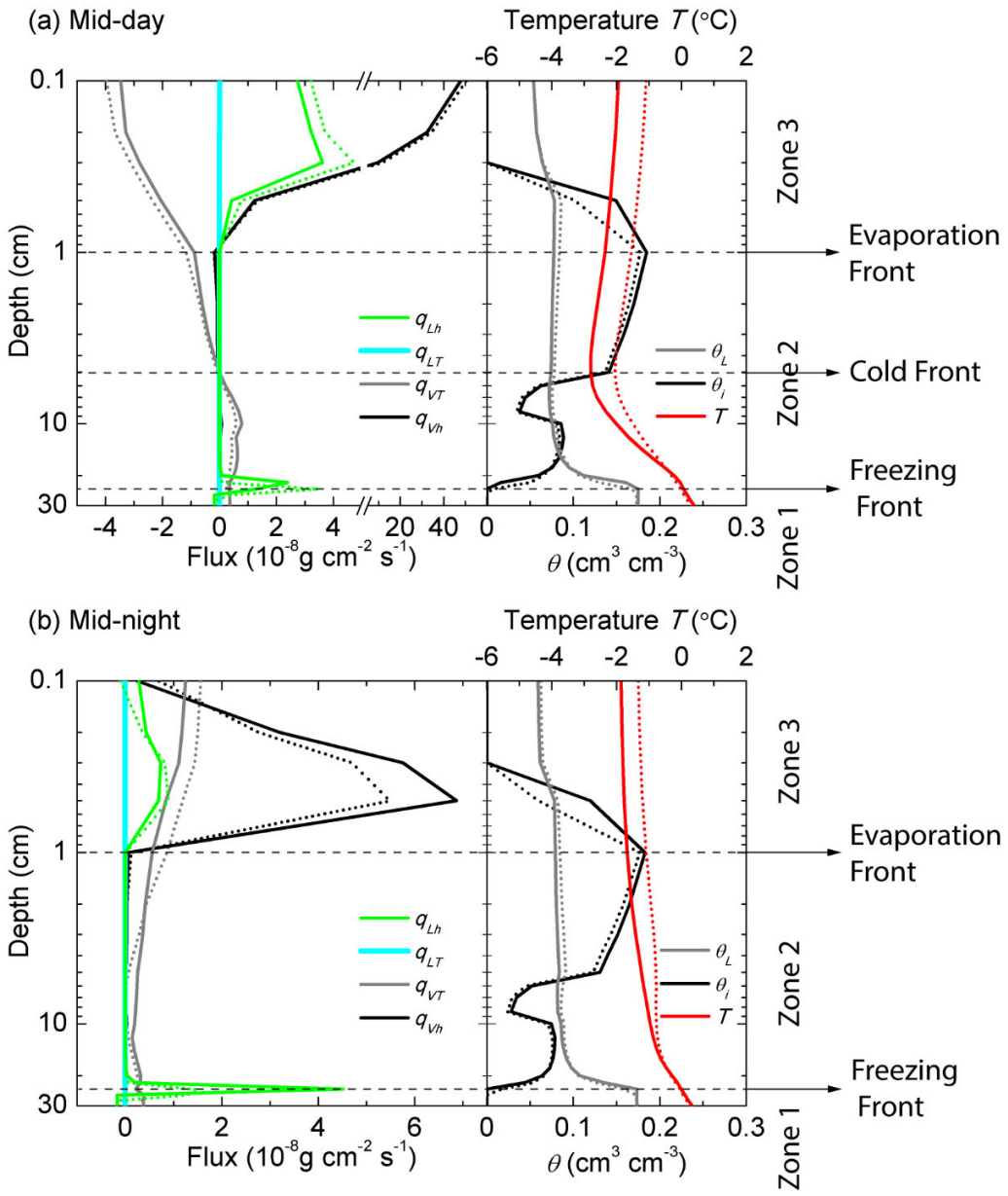

Figure S5.2. Simulated vertical profiles of the thermal and isothermal liquid water and vapor fluxes, soil ice content at 1200 and 0000 h of a typical freezing period during 11th and 12th Days after Dec. 1. 2015. Positive/negative values indicate upward/downward fluxes. Solid lines and dot lines represent for the fluxes and soil moisture, temperature and ice content profile on the 11th and 12th Days after Dec. 1. 2015, respectively.

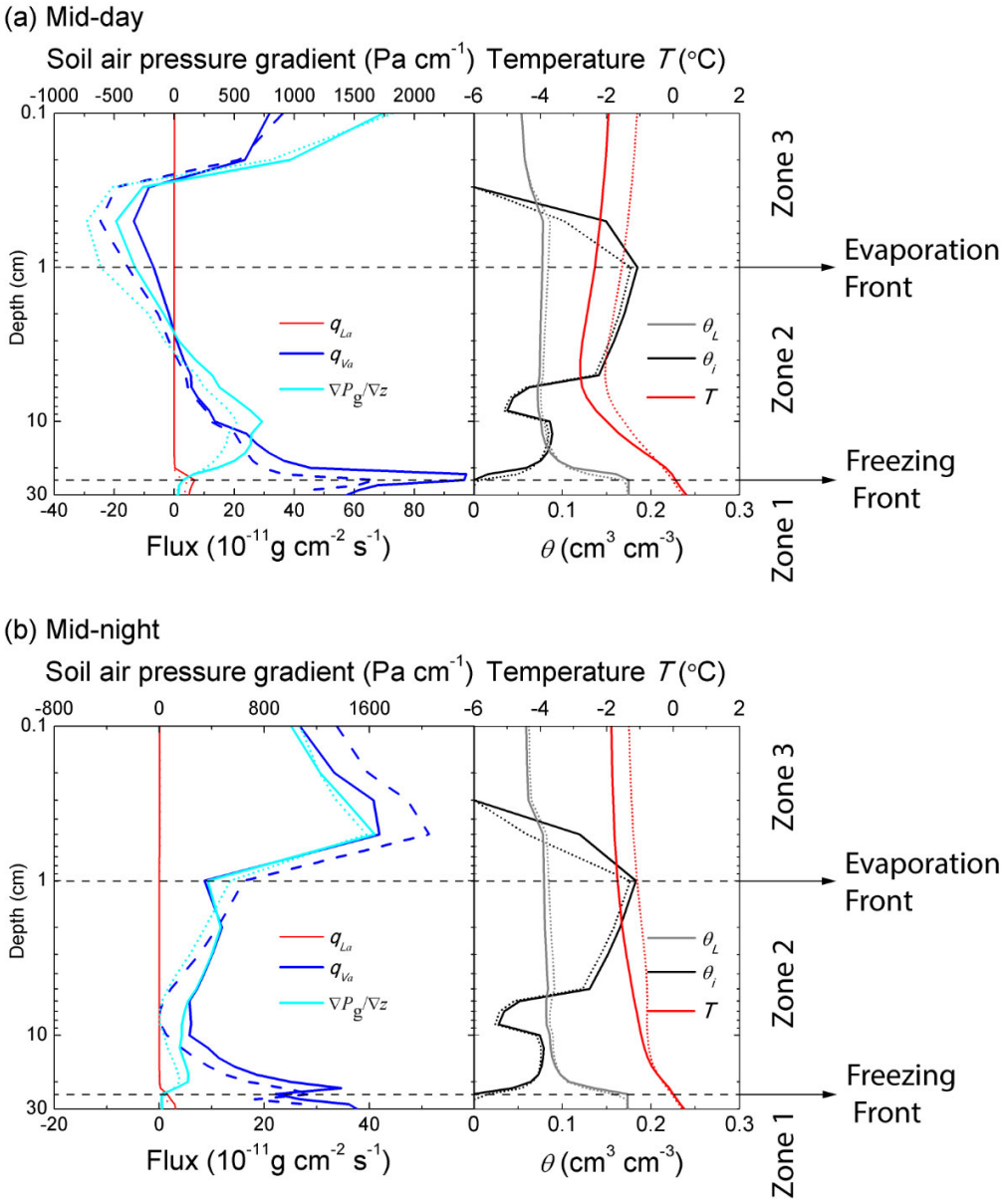

Figure S5.3. Simulated vertical profiles of the air pressure induced liquid water and vapor fluxes, soil air pressure gradient, soil ice content, liquid water content and soil temperature at 1200 and 0000 h of a typical freezing period during 11th and 12th Days after Dec. 1. 2015. Positive/negative values indicate upward/downward fluxes. Solid lines and dot lines represent for the fluxes and soil moisture, temperature and ice content profile on the 11th and 12th Days after Dec. 1. 2015, respectively.

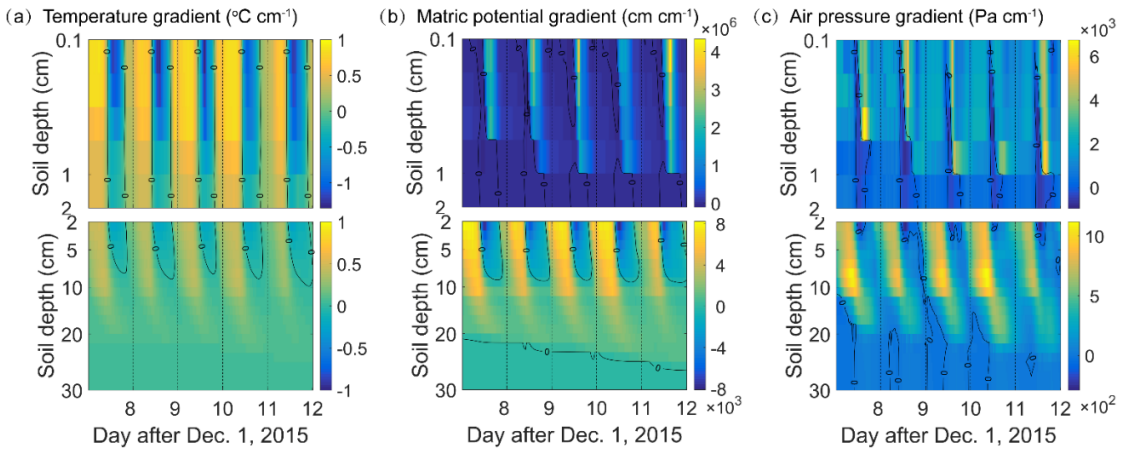

Figure S5.4. Spatial and temporal variations of (a) temperature gradient, (b) matric potential gradient and (c) air pressure gradient at surface soil layers (top 2cm, upper figure) and deeper soil layers (2-30cm, bottom figure), respectively, of a typical freezing period during 8th and 12th Days after Dec. 1. 2015.

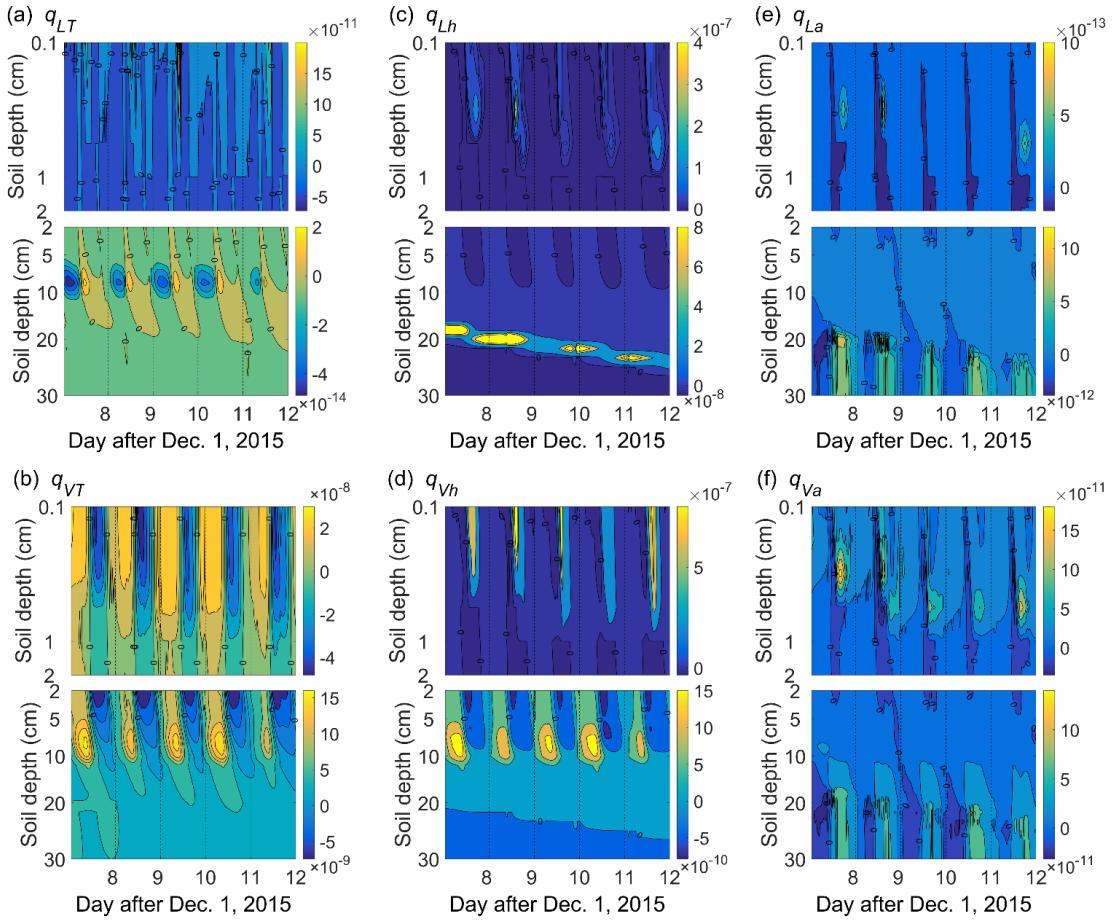

Figure S5.5. The spatial and temporal distributions of (a, and b) thermal liquid water, and vapor fluxes, (c, and d) isothermal liquid water, and vapor fluxes, (e, and f) advective liquid water, and vapor fluxes, at surface soil layers (top 2cm, upper figure) and deeper soil layers (2-30cm, bottom figure), respectively, of a typical freezing period during 8th and 12th Days after Dec. 1. 2015. Note that the unit for the fluxes is g cm^{-2} s^{-1}.

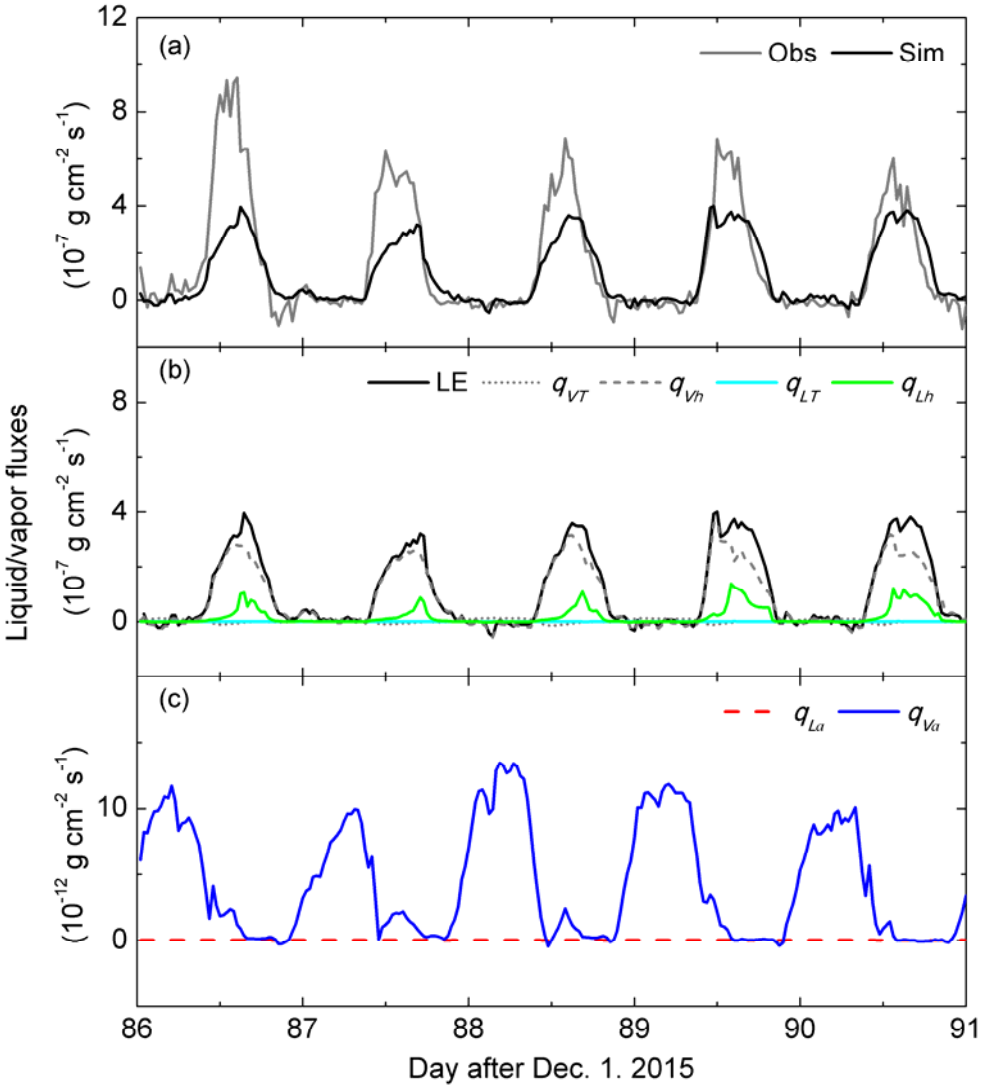

Figure S5.6. Same as Figure S5.1 but for a typical five-day thawing period (from 87th to 91th Days after Dec. 1. 2015).

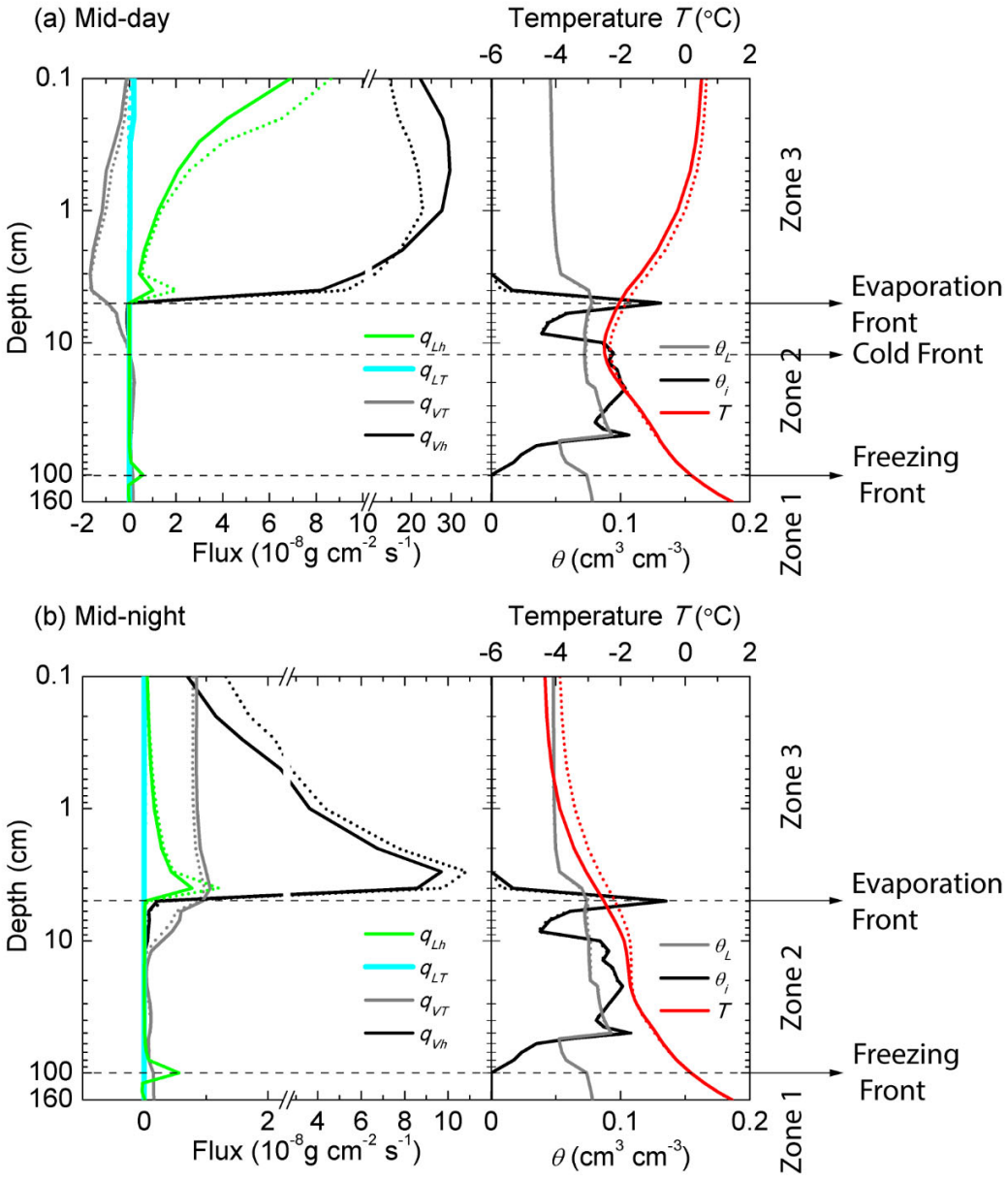

650

Figure S5.7. Simulated vertical profiles of the thermal and isothermal liquid water and vapor fluxes, soil ice content at 1200 and 0000 h of a typical freezing period during 90th and 91st Days after Dec. 1. 2015. Positive/negative values indicate upward/downward fluxes. Solid lines and dot lines represent for the fluxes and soil moisture, temperature and ice content profile on the 90th and 91st Days after Dec. 1. 2015,
655 respectively.

S5.2 Heat budget analysis

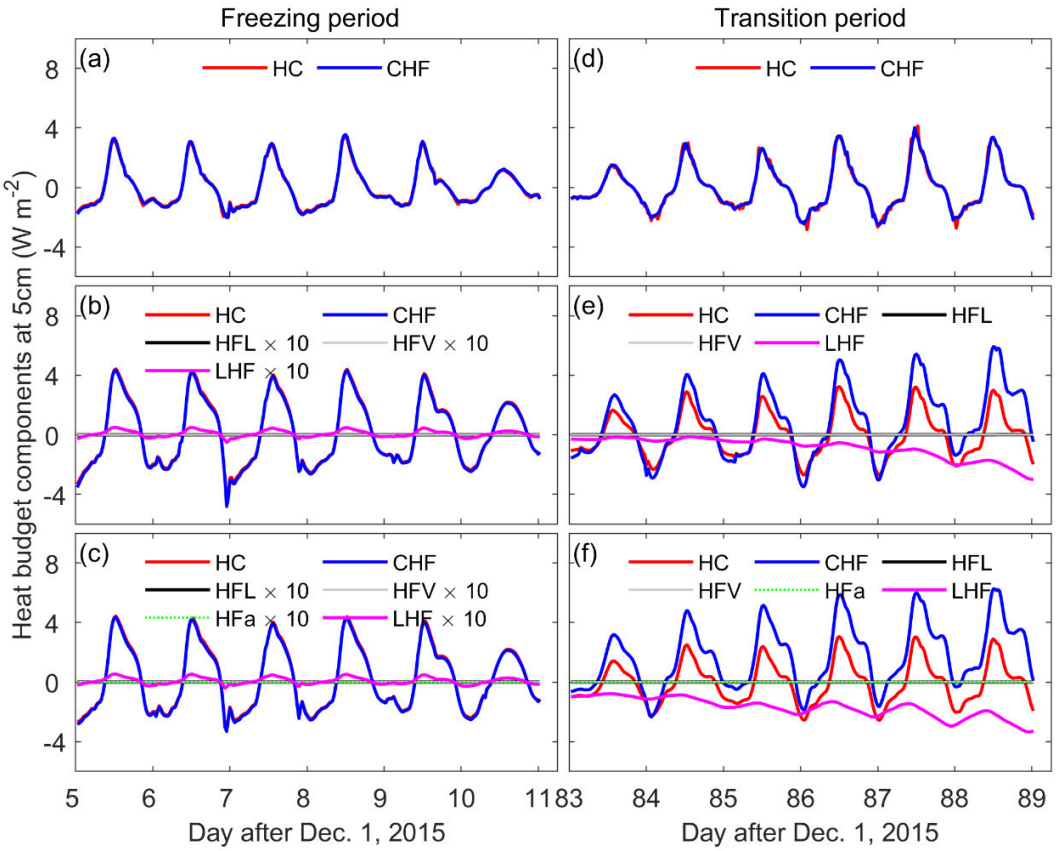

Figure S5.8. Time series of model simulated heat budget components at the soil depth of 5cm using (a &d) Basic Coupled Model (BCM), (b &e) Advanced Coupled Model (ACM), and (c &f) Advanced Coupled Model with Air flow (ACM-AIR) simulations during the typical 6-day freezing (left column) and freezing-thawing transition (right column) periods. HC, change rate of heat content, CHF, conductive heat flux divergence, HFL, convective heat flux divergence due to liquid water flow, HFV, convective heat flux divergence due to water vapor flow, HFa, convective heat flux divergence due to air flow, LHF, latent heat flux divergence. Note that for graphical purposes, HFL, HFV, HFa, and LHF were enhanced by a factor of 10 during the freezing period.

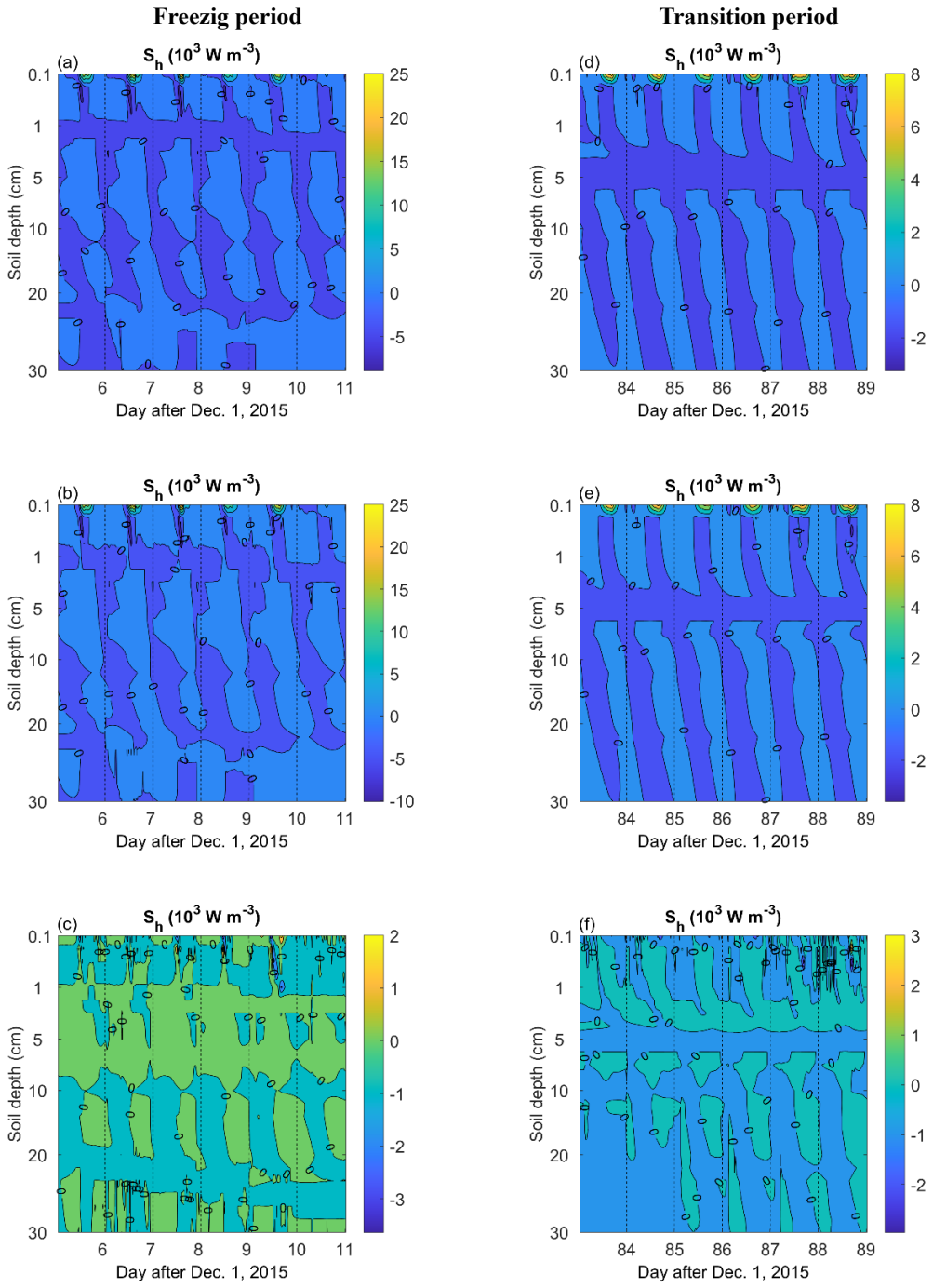

Figure S5.9. The spatial and temporal distributions of model estimated soil latent heat flux density using (a &d) Advanced Coupled Model (ACM), (b &e) Advanced Coupled Model with Air flow (ACM-AIR) and (c &f) the difference between ACM and ACM-AIR simulations ($S_{h,ACM-AIR} - S_{h,ACM}$) during the typical 6-day freezing and freezing-thawing transition periods. The left and right column are for the freezing and freezing-thawing transition period, respectively. Note that figures for the Basic Coupled Model (BCM) are absent as it can not simulate the subsurface soil latent heat flux density.

S6 Supplemental tables and figures

Table S6.1. The description of measurements and its temporal resolution deployed as inputs/outputs of the model (Maqu case)

Model/Measurements		Time Period	Time Interval	Notes
Meteorological Inputs	Precipitation	2015/12/1 - 2016/3/15	3 hourly	From weather station, about 12 km away from the study site. In order to meet the input requirement for the adaptive time step simulation, the precipitation was evenly distributed within the three hours.
	Air Temperature	2015/12/1 - 2016/3/15	30 min	From the in situ meteorological station. The time disaggregated values, to meet the requirement for the adaptive time step simulation (1 s - 30 mins), were obtained by the linear interpolation between the half-hour measurements.
	Air Relative Humidity	2015/12/1 - 2016/3/15	30 min	From the in situ meteorological station. The time disaggregated values, to meet the requirement for the adaptive time step simulation (1 s - 30 mins), were obtained by the linear interpolation between the half-hour measurements.
	Wind Speed	2015/12/1 - 2016/3/15	30 min	From the in situ meteorological station. The time disaggregated values, to meet the requirement for the adaptive time step simulation (1 s - 30 mins), were obtained by the linear interpolation between the half-hour measurements.
	Air pressure	2015/12/1 - 2016/3/15	30 min	From the in situ meteorological station. The time disaggregated values, to meet the requirement for the adaptive time step simulation (1 s - 30 mins), were obtained by the linear interpolation between the half-hour measurements.
	Four component downwelling and upwelling solar and thermal radiation	2015/12/1 - 2016/3/15	30 min	From the in situ meteorological station. The time disaggregated values, to meet the requirement for the adaptive time step simulation (1 s - 30 mins), were obtained by the linear interpolation between the half-hour measurements.
Model	STEMMUS/UEB	2015/12/1 - 2016/3/15	From 1 s to 30 mins	For all simulations, the adaptive time step was deployed.
Outputs	Soil Moisture	2015/12/1 - 2016/3/15	15 min	From the in situ 5TM ECH2O sensors, installed at 5 cm, 10 cm, 20 cm, 40 cm and 80 cm.
	Soil Temperature	2015/12/1 - 2016/3/15	15 min	From the in situ 5TM ECH2O sensors, installed at 5 cm, 10 cm, 20 cm, 40 cm and 80 cm.
	Albedo	2015/12/1 - 2016/3/15	30 min	The albedo was derived as the ration of half-hourly upwelling shortwave radiation to downwelling shortwave radiation measurements. The data during the nighttime was filtered out.
	Latent heat flux	2015/12/1 - 2016/3/15	30 min	From the installed Eddy Covariance (EC150) system

Table S6.2. Model parameters used for all simulations

Parameter	Unit	Value		Remarks
		Maqu case	Yakou case	
Soil Clay content	%	9.00 @ 0-10 cm; 10.12 @ 10-40 cm; 5.59 @ 40-160 cm	9.00 @ 0-10 cm; 10.60 @ 10-40 cm; 8.30 @ 40-160 cm	Soil texture, site-specific (can be obtained from the in-situ measurements, global soil texture maps)
Soil sand content	%	44.13 @ 0-10 cm; 44.27 @ 10-40 cm; 65.55 @ 40-160 cm	38.80 @ 0-10 cm; 44.30 @ 10-40 cm; 54.56 @ 40-160 cm	
Soil saturated conductivity K_s	10^{-6} m s^{-1}	1.45 @ 0-10 cm; 0.94 @ 10-40 cm; 0.68 @ 40-160 cm	0.645 @ 0-10 cm; 0.303 @ 10-40 cm; 0.103 @ 40-160 cm	Soil hydraulic parameters, site-specific (can be obtained from in-situ/laboratory measurements, or derived from soil texture information)
Soil saturated volumetric content θ_s	m^3 m^{-3}	0.5	0.45	
Soil residual water content θ_r	m^3 m^{-3}	0.035	0.010	
Air entry value	m^{-1}	0.041	0.0041	
VG fitting parameter n	-	1.332	1.365	
Specific heat of water	KJ Kg^{-1} K^{-1}	4.18	4.18	
Specific heat of ice	KJ Kg^{-1} K^{-1}	2.09	2.09	
Specific heat of air	KJ Kg^{-1} K^{-1}	1.005	1.005	Thermal properties of soil constituents, Constant
Water heat conductivity	W m^{-1} K^{-1}	0.6	0.6	
Ice heat conductivity	W m^{-1} K^{-1}	2.2	2.2	
Air heat conductivity	W m^{-1} K^{-1}	0.026	0.026	
Temperature threshold for rainfall	°C	3.5	5.0	Partition precipitation, can be adjusted
Temperature threshold for snowfall	°C	0	0	
Snow density	Kg/m^3	450	450	For the calculation of meltwater outflow, default value
Snow emissivity	-	0.99	0.99	Snow energy balance components, default value
Reflectance for new snow at visual bands	-	0.95	0.95	For the calculation of snow albedo, calibrated locally
Reflectance for new snow at near-infrared bands	-	0.65	0.65	
Snow surface roughness	m	0.001	0.0001	For the calculation of energy balance components, calibrated locally
Snow saturated hydraulic conductivity	m h^{-1}	160	160	For the calculation of the meltwater outflow, calibrated
Snow surface thermal conductance	m h^{-1}	0.02	0.02	For the calculation of snow energy balance components, default value
Thermally active depth of soil	m	0.4	0.4	For the calculation of snow energy balance components, default value

Table S6.3. A general overview of Utah energy balance (UEB) snowmelt model related research from the perspective of model development and applications

Study	Research aim, modelling/application perspective	Method/Data used	Study region	Model capability/utilities/focus/highlights
UEB model development/extension				
Tarboton et al. (1995); Tarboton and Luce (1996)	Developing a distributed snowmelt model UEB	Meteorological inputs: air temperature, wind speed, humidity, precipitation and total incoming solar and longwave radiation; site information	Central Sierra Snow Laboratory, California, USA; Reynolds Creek Experimental Watershed, Boise Idaho, USA; and the Utah State University drainage and evapotranspiration research farm, Logan, Utah, USA	Snow surface temperature, bulk temperature, snow water equivalent, melt outflow; snow sublimation/ablation,
Hellstrom (2000)	Developing the forest cover algorithms in UEB and test its performance for coniferous and deciduous forest	Meteorological inputs; canopy architecture measurements: vegetation area index (VAI), sky view factor (SVF), forest canopy closure (FC); site information	Northern Michigan, USA	Canopy processes including attenuation of solar radiation and wind speed, the mixed sky and canopy components of longwave irradiance, and precipitation interception by canopy elements; more realistic atmospheric stability algorithm,
Mahat and Tarboton (2012)	Better estimating the radiation energy within and beneath the forest canopy in UEB	Meteorological inputs, vegetation properties, site information	Rocky Mountains in Utah, USA	Two stream radiation transfer model that explicitly accounts for canopy scattering, absorption and reflection,
Mahat and Tarboton (2014)	Representing the canopy snow interception, unloading and melt in UEB	Meteorological inputs, vegetation properties, site information	Rocky Mountains in Utah, USA	New UEB model algorithms that represent the processes of canopy snow interception, sublimation, mass unloading and melt,
You et al. (2014)	Improve snow surface temperature modelling	Meteorological inputs; site information	Central Sierra Snow Laboratory, CA, Utah State University experimental farm, USA, and subnivean snow laboratory at Niwot Ridge, USA	Modified force-restore approach; adjust effective conductivity considering the presence of ground near to a shallow snow surface; representing the penetration of the refreezing front following melt,
Sen Gupta et al. (2015)	Developing a modelling framework facilitating the integration of UEB, hydrologic model BASINS, and GeoSFM	Gridded meteorological forcing, DEM, vegetation variables, land cover, glacier outlines and albedo, hydrological data	Langtang Khola watershed (Himalaya), Nepal	Hydrological model with topographical effect, surface water and streamflow,
Gichamo and Tarboton (2019)	Coupling UEB to hydrologic model SAC-SMA together with assimilation of snow and streamflow observations	Gridded meteorological forcing, vegetation properties, watershed domain variables (e.g., slope, aspect), hydrological data, and SWE & discharge data for assimilation	Green River watershed, Salt Lake City, USA	UEB snowmelt model with assimilation of SWE using ensemble Kalman filter, Sacramento Soil Moisture Accounting (SAC-SMA), rutpix7 stream routing model with assimilation of streamflow observation using particle filter,
Gichamo and Tarboton (2020)	Developing UEB parallel for the simulation of snow process using parallel computing	Gridded meteorological forcing, vegetation properties, watershed domain variables (e.g., slope, aspect), in NetCDF format	Logan River watershed, Utah, USA	Two parallel versions of UEB model, one using the Message Passing Interface (MPI) and the other using NVIDIA's CUDA code on Graphics Processing Unit (GPU),
UEB model applications				
(Gardiner et al., 1998)	Testing UEB in terms of SWE	Meteorological inputs, site information	Paternoster Valley, Signy Island, South Orkney Islands, Antarctic	First application of UEB in Antarctic,
Schulz and de Jong (2004)	Testing UEB in terms of snowmelt and sublimation	Meteorological variables, site information	High Atlas Mountains of Morocco, Morocco	Snowmelt and sublimation/ablation,
Brown et al. (2014)	Estimating the contribution of glacier and snowmelt to stream flow using integrated modelling system (UEB,	Downscaled NASA satellite based and earth system data products, in-situ hydrologic data	Langtang Khola watershed (Himalaya), Nepal	UEB considering glacier ice melt over clean and debris-covered tongues, Geospatial Stream Flow Model (GeoSFM), BASINS model, streamflow,

	GeoSFM, BASINS)			
Sultana et al. (2014)	Resolve the underestimation of SWE by Noah 2.7.1 by incorporating UEB	Meteorological forcing from NLDAS-2, site information	NRCS SNOTEL stations, California, USA; T.W. Daniel Experimental Forest site, Utah, USA	Snow surface temperature, snowmelt event, SWE,
Pimentel et al. (2015)	Improving snow cover simulation over mountainous regions with highly irregular distribution	High-frequency images were combined with UEB model to reproduce snow evolution at cell scale (30 m × 30 m) by means of the assimilation of the snow cover fraction observation dataset obtained from terrestrial photography	Sierra Nevada, southern Spain	Terrestrial photography, data assimilation of snow cover observation; Snow cover and snow depth,
Raleigh et al. (2015)	Diagnosing the sensitivity/impact of forcing error characteristics on snow simulations	Site information, meteorological forcing with various error characteristics	Imnavait Creek site in Alaska, USA; the maritime Col de Porte site in the Rhône-Alpes of France, France; the intermountain Reynolds Mountain East sheltered site in the Owyhee Range in Idaho, USA; the continental Swamp Angel Study Plot site in the San Juan Mountains of Colorado, USA	Sobol's global sensitivity analysis,
Watson et al. (2006)	Testing distributed UEB	Daily precipitation and temperature data, and 28.5-m maps of mean annual precipitation, terrain, vegetation, and geothermal heat flux	SNOTEL sites, USA	Spatial SWE, requires improvements of snow interception, and snowpack thermal dynamics for tested regions,
Khanduri and Thakur (2020)	Testing UEB in terms of snowmelt runoff	Meteorological data and remotely sensed data from Landsat ETM+, IRS P-6 LISS-III and MODIS 8-day snow cover data product	Himachal Pradesh state, India	Snowmelt runoff,
Liu et al. (2020)	Testing UEB in terms of glacier- and snowmelt-driven streamflow	Spatial downscaling of the China meteorological forcing dataset (CMFD) coupled with other parameters, the model simulates the total surface water balance using surface water input from snowmelt, glacial melt and rainfall	Middle Tianshan Mountains, China	A glacier melt model and snow above/below the forest ablation algorithm, streamflow.

Table S6.4. The identification of snowpack using the direct evidence, i.e., the observed soil water equivalent (SWE, shaded with yellow color) and the indirect method, i.e., the albedo variation together with the ancillary meteorological data (air temperature Ta and precipitation) (shaded with blue color). The observed snow water equivalent is in 6-hour interval.

Time	Ta (°C)	Precipitation (mm)	Albedo	SWE (mm)	Remarks
2016-10-10 12:30:00	-0.8	0	0.14		
2016-10-10 18:30:00	-1.59	0	0.36		
2016-10-11 00:30:00	-5.24	0			
2016-10-11 06:30:00	-6.73	0		10.90	
2016-10-11 12:30:00	-2.97	0.4	0.87	11.98	
2016-10-11 18:30:00	-4.02	0	0.99	13.42	
2016-10-12 00:30:00	-4.44	0		15.42	First example period
2016-10-12 06:30:00	-5.19	0		16.74	
2016-10-12 12:30:00	-3	0	0.62	17.22	
2016-10-12 18:30:00	-1.45	0	0.61	17.17	
2016-10-13 00:30:00	-2.84	0		16.30	
2016-10-13 06:30:00	-5.14	0		15.61	
2016-10-13 12:30:00	-0.37	0	0.18		
2017-01-28 12:30:00	-13.7	0	0.19		
2017-01-28 18:30:00	-14.32	0			
2017-01-29 00:30:00	-17.1	0			
2017-01-29 06:30:00	-15.15	0		2.51	
2017-01-29 12:30:00	-12.32	0	0.64	4.59	
2017-01-29 18:30:00	-9.76	0		6.69	
2017-01-30 00:30:00	-11.82	0		8.09	
2017-01-30 06:30:00	-12.68	0		9.26	
2017-01-30 12:30:00	-8.95	0	0.61	8.69	
2017-01-30 18:30:00	-9.58	0	0.95	8.31	
2017-01-31 00:30:00	-11.71	0		7.84	
2017-01-31 06:30:00	-13.47	0		7.01	
2017-01-31 12:30:00	-10.24	0	0.51	7.18	Second example period
2017-01-31 18:30:00	-9.76	0	0.85	6.40	
2017-02-01 00:30:00	-11.95	0		5.93	
2017-02-01 06:30:00	-15.5	0		4.75	
2017-02-01 12:30:00	-10.63	0	0.41	4.71	
2017-02-01 18:30:00	-8.66	0		5.86	
2017-02-02 00:30:00	-10.58	0		6.12	
2017-02-02 06:30:00	-12.15	0		5.85	
2017-02-02 12:30:00	-9.47	0	0.32	4.49	
2017-02-02 18:30:00	-8.17	0		3.82	
2017-02-03 00:30:00	-10.22	0		4.27	
2017-02-03 06:30:00	-12.4	0		4.27	
2017-02-03 12:30:00	-7.69	0	0.29	4.00	

2017-02-03 18:30:00	-7.73	0	0.23	4.06	
2017-02-04 00:30:00	-8.59	0		3.50	
2017-02-04 06:30:00	-8.37	0		2.08	
2017-02-04 12:30:00	-5.59	0	0.23		
2017-02-06 12:30:00	-2.91	0	0.19		
2017-02-06 18:30:00	-13.13	0	0.49		
2017-02-07 00:30:00	-17.7	0			
2017-02-07 06:30:00	-19.04	0			
2017-02-07 12:30:00	-16.09	0	0.30	1.90	
2017-02-07 18:30:00	-17.33	0	0.77	2.52	
2017-02-08 00:30:00	-18.17	0		3.54	
2017-02-08 06:30:00	-18.25	0		4.61	
2017-02-08 12:30:00	-13.95	0		5.73	
2017-02-08 18:30:00	-15.16	0	0.99	7.19	
2017-02-09 00:30:00	-17.3	0		7.44	
2017-02-09 06:30:00	-17.53	0		7.74	
2017-02-09 12:30:00	-13.56	0	0.65	7.91	
2017-02-09 18:30:00	-12.43	0		7.64	
2017-02-10 00:30:00	-16.64	0		8.12	
2017-02-10 06:30:00	-17.43	0		7.71	
2017-02-10 12:30:00	-16.36	0	0.87	5.99	
2017-02-10 18:30:00	-14.38	0		7.58	
2017-02-11 00:30:00	-16.07	0		8.05	
2017-02-11 06:30:00	-16.7	0		8.54	Third example period
2017-02-11 12:30:00	-11.54	0	0.61	8.92	
2017-02-11 18:30:00	-10.01	0		8.93	
2017-02-12 00:30:00	-13.76	0		8.27	
2017-02-12 06:30:00	-15.37	0		8.03	
2017-02-12 12:30:00	-9.63	0	0.59	7.02	
2017-02-12 18:30:00	-7.45	0	0.93	6.61	
2017-02-13 00:30:00	-9.27	0		6.37	
2017-02-13 06:30:00	-12.22	0		5.83	
2017-02-13 12:30:00	-7.75	0	0.51	5.71	
2017-02-13 18:30:00	-9.31	0	0.88	5.79	
2017-02-14 00:30:00	-11.14	0		5.61	
2017-02-14 06:30:00	-14.02	0		5.51	
2017-02-14 12:30:00	-8.78	0	0.46	5.55	
2017-02-14 18:30:00	-7.36	0		4.80	
2017-02-15 00:30:00	-10.56	0		4.61	
2017-02-15 06:30:00	-12.26	0		4.52	
2017-02-15 12:30:00	-7.71	0	0.37	3.99	
2017-02-15 18:30:00	-3.45	0	0.76	3.81	
2017-02-16 00:30:00	-6.3	0		2.03	

2017-02-16 06:30:00	-7.07	0		2.62
2017-02-16 12:30:00	-9.74	0	0.29	2.33
2017-02-16 18:30:00	-10.48	0		1.78
2017-02-17 00:30:00	-10.66	0		1.88
2017-02-17 06:30:00	-10.74	0		2.05
2017-02-17 12:30:00	-7.3	0	0.25	2.12
2017-02-17 18:30:00	-4.69	0	0.57	
2017-02-18 00:30:00	-6.31	0		
2017-02-18 06:30:00	-8.64	0		1.26
2017-02-18 12:30:00	-5.53	0	0.21	

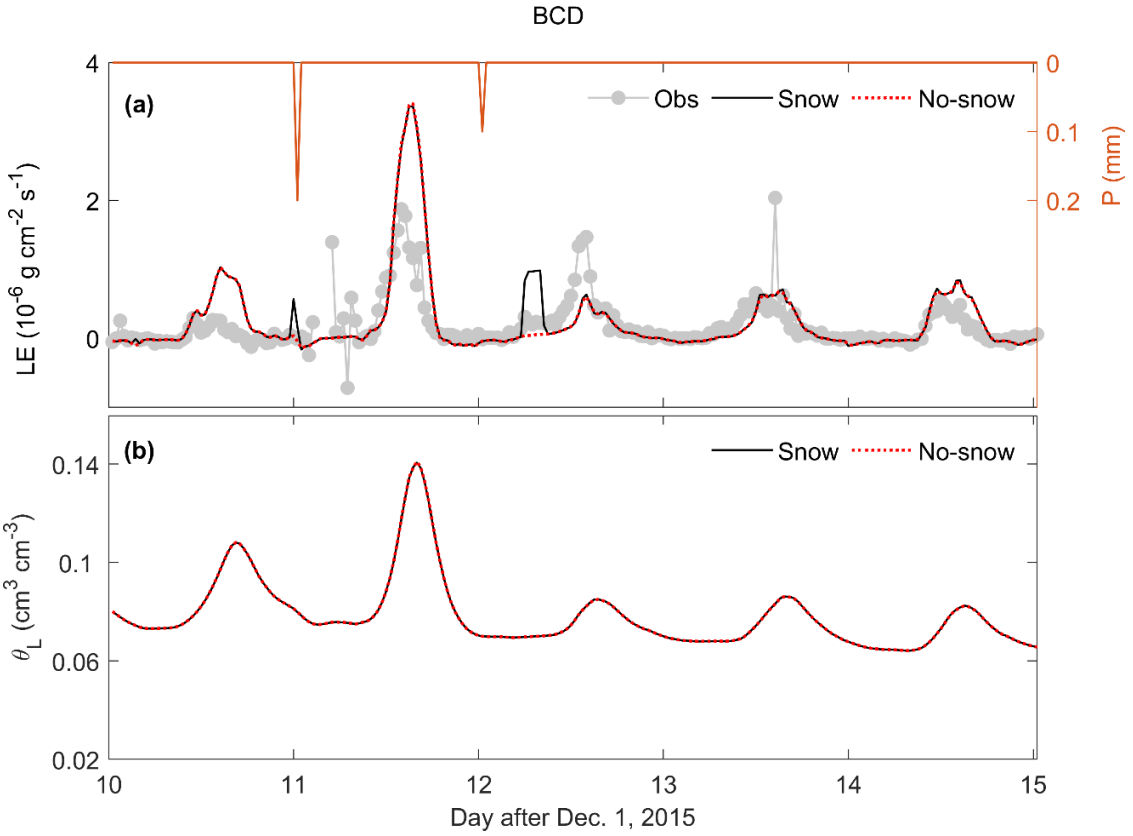
BCD
(a)
Obs
Snow
No-snow
LE (10^{-6} g cm^{-2} s^{-1})
P (mm)
(b)
Snow
No-snow
θ_L (cm^3 cm^{-3})
Day after Dec. 1, 2015

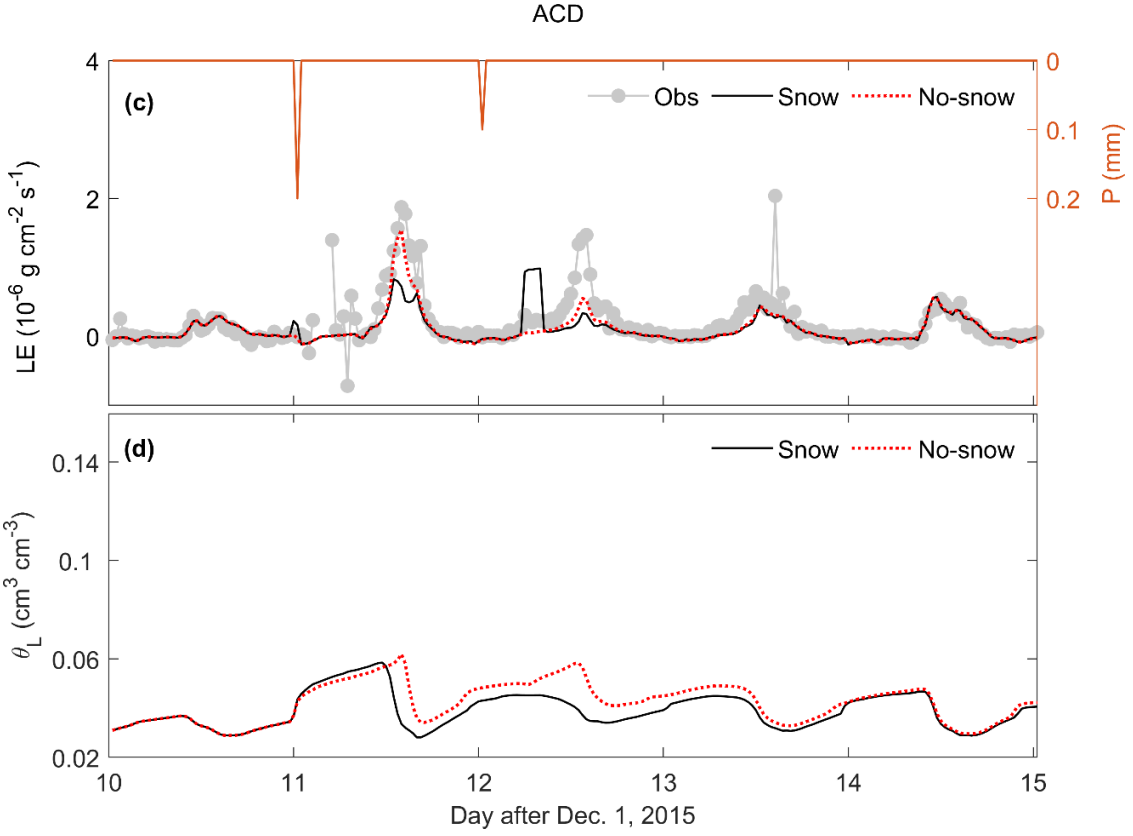
ACD
(c)
Obs
Snow
No-snow
LE (10^{-6} g cm^{-2} s^{-1})
P (mm)
(d)
Snow
No-snow
θ_L (cm^3 cm^{-3})
Day after Dec. 1, 2015

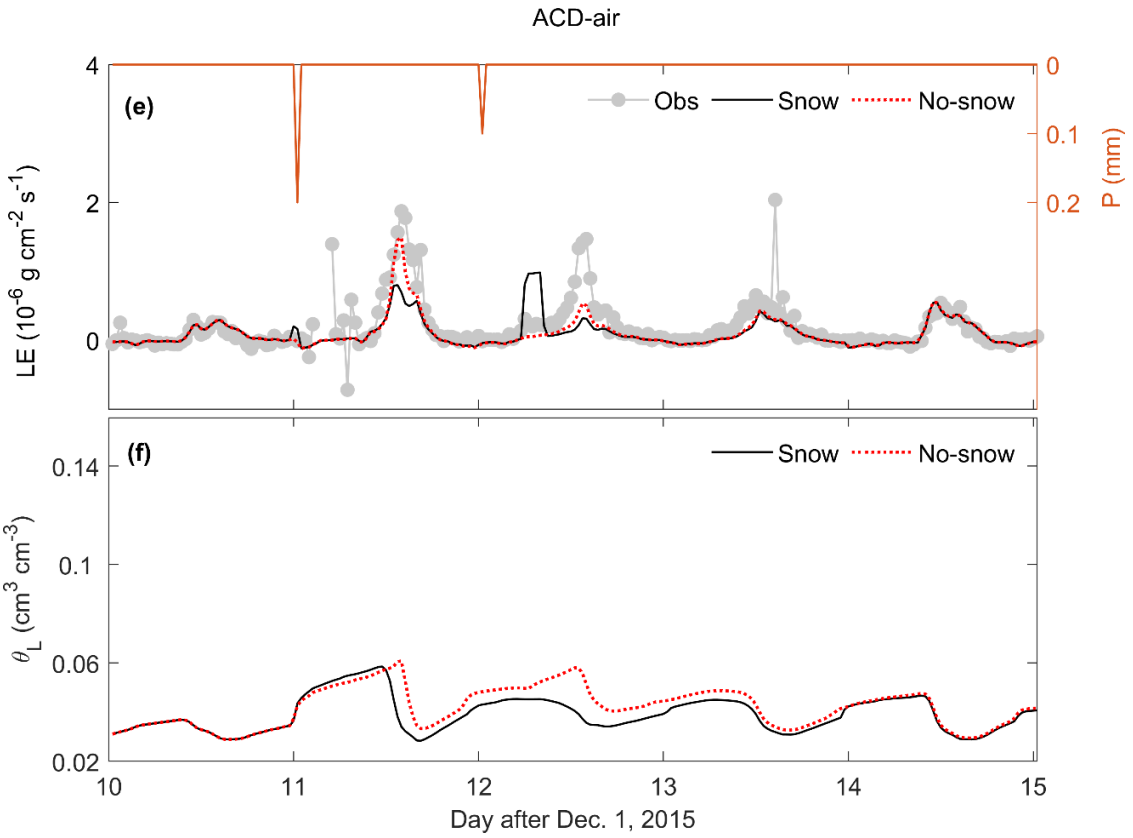

Figure S6.1. Observed latent heat flux and simulated (a, c &e) latent heat flux and (b, d &f) surface soil liquid water content θ_L with/without snow module of a typical five-day freezing period (from 10th to 15th Day after Dec. 1. 2015) with precipitation. LE is the latent heat flux.

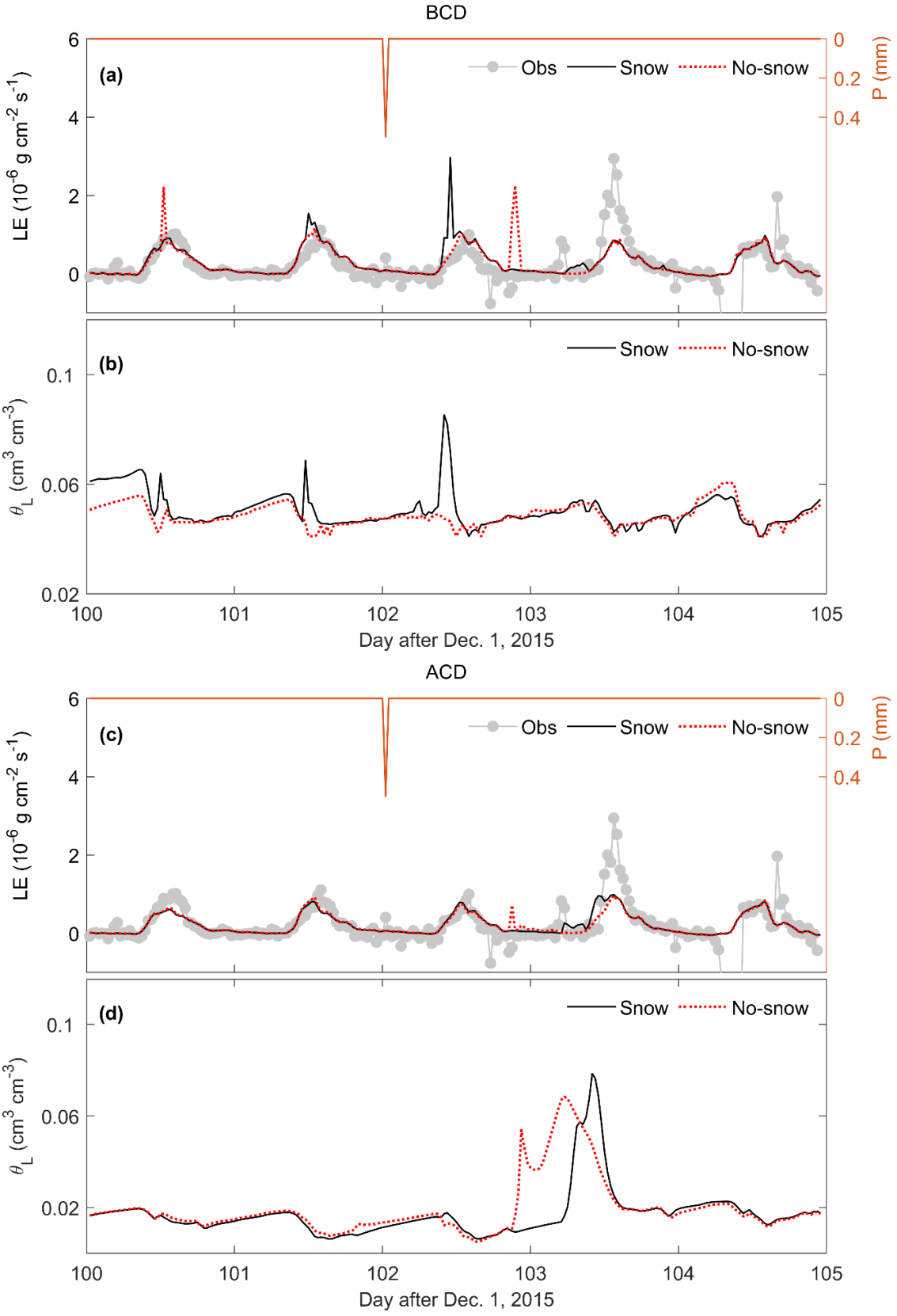
BCD
(a)
Obs
Snow
No-snow
LE (10^{-6} g cm^{-2} s^{-1})
P (mm)
(b)
θ_L (cm^3 cm^{-3})
Day after Dec. 1, 2015
ACD
(c)
(d)

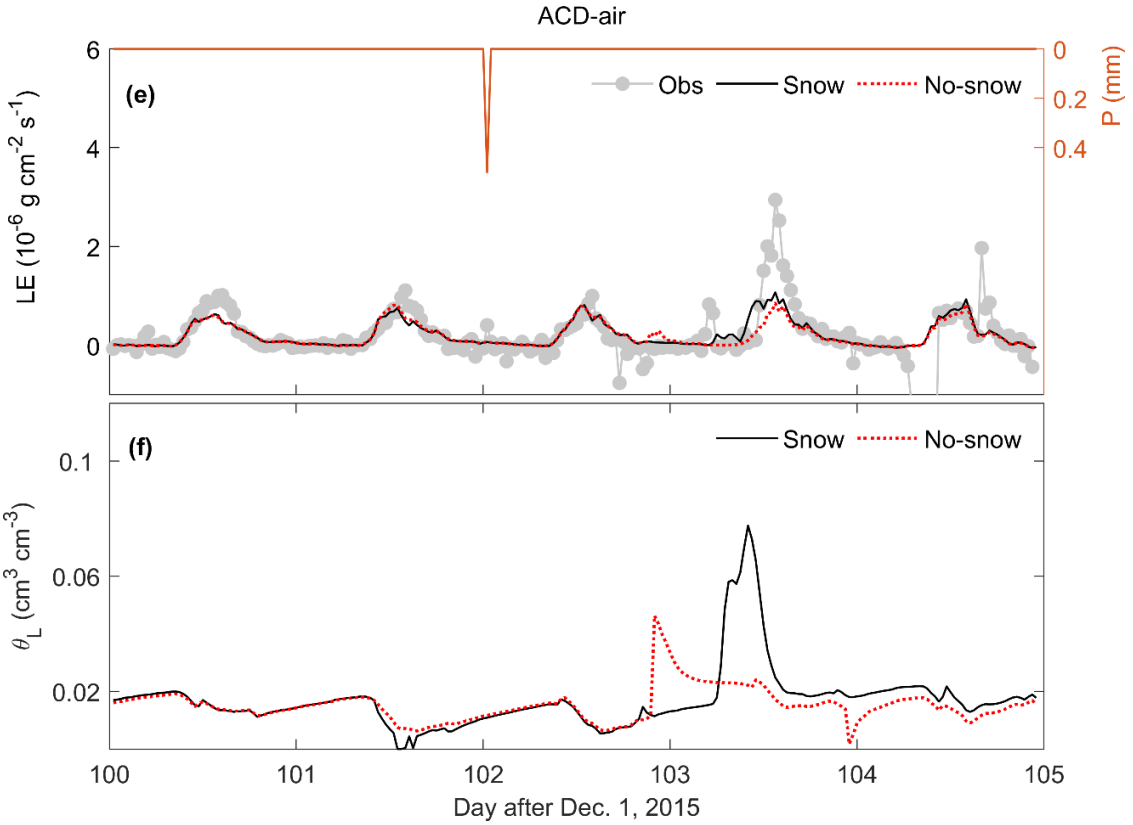

Figure S6.2. Observed latent heat flux and simulated (a, c &e) latent heat flux and (b, d &f) surface soil liquid water content θ_L with/without snow module of a typical five-day thawing period (from 100th to 105th Day after Dec. 1. 2015) with precipitation. LE is the latent heat flux.

Reference

Brown, M. E., Racoviteanu, A. E., Tarboton, D. G., Gupta, A. S., Nigro, J., Policelli, F., Habib, S., Tokay, M., Shrestha, M. S., Bajracharya, S., Hummel, P., Gray, M., Duda, P., Zaitchik, B., Mahat, V., Artan, G., and Tokar, S.: An integrated modeling system for estimating glacier and snow melt driven streamflow from remote sensing and earth system data products in the Himalayas, J Hydrol, 519, 1859-1869, https://doi.org/10.1016/j.jhydrol.2014.09.050, 2014.

Clapp, R. B., and Hornberger, G. M.: Empirical equations for some soil hydraulic properties, Water Resour Res, 14, 601-604, https://doi.org/10.1029/WR014i004p00601, 1978.

Clark, M. P., Nijssen, B., Lundquist, J. D., Kavetski, D., Rupp, D. E., Woods, R. A., Freer, J. E., Gutmann, E. D., Wood, A. W., Brekke, L. D., Arnold, J. R., Gochis, D. J., and Rasmussen, R. M.: A unified approach for process-based hydrologic modeling: 1. Modeling concept, Water Resour Res, 51, 2498-2514, https://doi.org/10.1002/2015wr017198, 2015.

Dall'Amico, M.: Coupled water and heat transfer in permafrost modeling, University of Trento, 2010.

De Vries, D. A.: Simultaneous transfer of heat and moisture in porous media, Eos, Transactions American Geophysical Union, 39, 909-916, https://doi.org/10.1029/TR039i005p00909, 1958.

de Vries, D. A.: Thermal properties of soils, Physics of Plant Environment, edited by: van Wijk, W. R., North-Holland Publishing Company, Amsterdam, 210-235 pp., 1963.

Dickinson, R. E., Henderson-Sellers, A., and Kennedy, P. J.: Biosphere-atmosphere Transfer Scheme (BATS) Version 1e as Coupled to the NCAR Community Climate Model (No. NCAR/TN-387+STR), University Corporation for Atmospheric Research, 1993.

Edlefsen, N., and Anderson, A.: Thermodynamics of soil moisture, Hilgardia, 15, 31-298, 1943.

Farouki, O. T.: The thermal properties of soils in cold regions, Cold Regions Sci Tech, 5, 67-75, https://doi.org/10.1016/0165-232X(81)90041-0, 1981.

Feddes, R. A., Kowalik, P. J., and Zaradny, H.: Simulation of field water use and crop yield, Centre for Agricultural Publishing and Documentation, Wageningen, the Netherlands, 189 pp., 1978.

Gale, M. R., and Grigal, D. F.: Vertical root distributions of northern tree species in relation to successional status, Canadian Journal of Forest Research, 17, 829-834, https://doi.org/10.1139/x87-131, 1987.

Gardiner, M. J., Ellis-Evans, J. C., Anderson, M. G., and Tranter, M.: Snowmelt modelling on Signy Island, South Orkney Islands, Ann Glaciol, 26, 161-166, https://doi.org/10.3189/1998aog26-1-161-166, 1998.

Gichamo, T. Z., and Tarboton, D. G.: Ensemble Streamflow Forecasting Using an Energy Balance Snowmelt Model Coupled to a Distributed Hydrologic Model with Assimilation of Snow and Streamflow Observations, Water Resour Res, 55, 10813-10838, https://doi.org/10.1029/2019wr025472, 2019.

Gichamo, T. Z., and Tarboton, D. G.: UEB parallel: Distributed snow accumulation and melt modeling using parallel computing, Environ Model Software, 125, https://doi.org/10.1016/j.envsoft.2019.104614, 2020.

Hansson, K., Šimůnek, J., Mizoguchi, M., Lundin, L. C., and van Genuchten, M. T.: Water flow and heat transport in frozen soil: Numerical solution and freeze-thaw applications, Vadose Zone J, 3, 693-704, 2004.

Hellstrom, R. A.: Forest cover algorithms for estimating meteorological forcing in a numerical snow model, Hydrol Processes, 14, 3239-3256, https://doi.org/10.1002/1099-1085(20001230)14:18<3239::aid-hyp201>3.0.co;2-o, 2000.

Jackson, R. B., Canadell, J., Ehleringer, J. R., Mooney, H. A., Sala, O. E., and Schulze, E. D.: A Global Analysis of Root Distributions for Terrestrial Biomes, Oecologia, 108, 389-411, 1996.

Johansen, O.: Thermal conductivity of soils, PhD, University of Trondheim, 236 pp., 1975.

Kay, B. D., and Groenevelt, P. H.: On the Interaction of Water and Heat Transport in Frozen and Unfrozen Soils: I. Basic Theory; The Vapor Phase, Soil Sci Soc Am J, 38, 395-400, https://doi.org/https://doi.org/10.2136/sssaj1974.03615995003800030011x, 1974.

Koopmans, R. W. R., and Miller, R. D.: Soil Freezing and Soil Water Characteristic Curves, Soil Sci Soc Am J, 30, 680-685, https://doi.org/10.2136/sssaj1966.03615995003000060011x, 1966.

Liu, Y., Xu, J. H., Lu, X. Y., and Nie, L.: Assessment of glacier- and snowmelt-driven streamflow in the arid middle Tianshan Mountains of China, Hydrol Processes, 34, 2750-2762, https://doi.org/10.1002/hyp.13760, 2020.

Mahat, V., and Tarboton, D. G.: Canopy radiation transmission for an energy balance snowmelt model, Water Resour Res, 48, https://doi.org/10.1029/2011WR010438, 2012.

Mahat, V., and Tarboton, D. G.: Representation of canopy snow interception, unloading and melt in a parsimonious snowmelt model, Hydrol Processes, 28, 6320-6336, https://doi.org/10.1002/hyp.10116, 2014.
Milly, P. C. D.: Moisture and heat transport in hysteretic, inhomogeneous porous media: A matric head-based formulation and a numerical model, Water Resour Res, 18, 489-498, https://doi.org/10.1029/WR018i003p00489, 1982.
Mualem, Y.: New model for predicting the hydraulic conductivity of unsaturated porous media, Water Resour Res, 12, 513-522, 1976.
Philip, J. R., and Vries, D. A. D.: Moisture movement in porous materials under temperature gradients, Eos, Transactions American Geophysical Union, 38, 222-232, https://doi.org/10.1029/TR038i002p00222, 1957.
Pimentel, R., Herrero, J., Zeng, Y., Su, Z., and Polo, M. J.: Study of Snow Dynamics at Subgrid Scale in Semiarid Environments Combining Terrestrial Photography and Data Assimilation Techniques, J Hydrometeorol, 16, 563-578, https://doi.org/10.1175/jhm-d-14-0046.1, 2015.
Prunty, L.: Soil water heat of transport, Journal of Hydrologic Engineering, 7, 435-440, 2002.
Raleigh, M. S., Lundquist, J. D., and Clark, M. P.: Exploring the impact of forcing error characteristics on physically based snow simulations within a global sensitivity analysis framework, Hydrol Earth Syst Sci, 19, 3153-3179, https://doi.org/10.5194/hess-19-3153-2015, 2015.
Richards, L. A.: Capillary Conduction of Liquids Through Porous Mediums, Physics, 1, 318, 1931.
Schulz, O., and de Jong, C.: Snowmelt and sublimation: field experiments and modelling in the High Atlas Mountains of Morocco, Hydrol Earth Syst Sci, 8, 1076-1089, https://doi.org/10.5194/hess-8-1076-2004, 2004.
Sen Gupta, A., Tarboton, D. G., Hummel, P., Brown, M. E., and Habib, S.: Integration of an energy balance snowmelt model into an open source modeling framework, Environ Model Software, 68, 205-218, https://doi.org/10.1016/j.envsoft.2015.02.017, 2015.
Sultana, R., Hsu, K. L., Li, J., and Sorooshian, S.: Evaluating the Utah Energy Balance (UEB) snow model in the Noah land-surface model, Hydrol Earth Syst Sci, 18, 3553-3570, https://doi.org/10.5194/hess-18-3553-2014, 2014.
Tarboton, D. G., Chowdhury, T. G., and Jackson, T. H.: A spatially distributed energy balance snowmelt model, Biogeochemistry of seasonally snow-covered catchments Proc symposium, Boulder, 1995, 228, 141-155, 1995.
Tarboton, D. G., and Luce, C. H.: Utah Energy Balance Snow Accumulation and Melt Model (UEB), Computer model technical description and users guide, Utah Water Research Laboratory and USDA Forest Service Intermountain Research Station, 1996.
Tarnawski, V. R., and Wagner, B.: A new computerized approach to estimating the thermal properties of unfrozen soils, Can Geotech J, 29, 714-720, https://doi.org/10.1139/t92-079, 1992.
Tarnawski, V. R., and Wagner, B.: Modeling the thermal conductivity of frozen soils, Cold Regions Sci Tech, 22, 19-31, https://doi.org/10.1016/0165-232X(93)90043-8, 1993.
Taylor, G. S., and Luthin, J. N.: A model for coupled heat and moisture transfer during soil freezing, Can Geotech J, 15, 548-555, https://doi.org/10.1139/t78-058, 1978.
Tian, Z., Lu, Y., Horton, R., and Ren, T.: A simplified de Vries-based model to estimate thermal conductivity of unfrozen and frozen soil, Eur J Soil Sci, 67, 564-572, https://doi.org/10.1111/ejss.12366, 2016.
Van Genuchten, M. T.: A closed-form equation for predicting the hydraulic conductivity of unsaturated soils, Soil Sci Soc Am J, 44, 892-898, https://doi.org/10.2136/SSSAJ1980.03615995004400050002X, 1980.
Vandegriend, A. A., and Owe, M.: BARE SOIL SURFACE-RESISTANCE TO EVAPORATION BY VAPOR DIFFUSION UNDER SEMIARID CONDITIONS, Water Resour Res, 30, 181-188, https://doi.org/10.1029/93wr02747, 1994.
Wang, Y., Zeng, Y., Yu, L., Yang, P., Van de Tol, C., Cai, H., and Su, Z.: Integrated Modeling of Photosynthesis and Transfer of Energy, Mass and Momentum in the Soil-Plant-Atmosphere Continuum System, Geosci Model Dev Discuss, 2020, 1-37, https://doi.org/10.5194/gmd-2020-85, 2020.
Watson, F. G. R., Newman, W. B., Coughlan, J. C., and Garrott, R. A.: Testing a distributed snowpack simulation model against spatial observations, J Hydrol, 328, 453-466, https://doi.org/10.1016/j.jhydrol.2005.12.012, 2006.
Yang, K., Chen, Y. Y., and Qin, J.: Some practical notes on the land surface modeling in the Tibetan Plateau, Hydrol Earth Syst Sci, 13, 687-701, https://doi.org/10.5194/hess-13-687-2009, 2009.
You, J., Tarboton, D. G., and Luce, C. H.: Modeling the snow surface temperature with a one-layer energy balance snowmelt model, Hydrol Earth Syst Sci, 18, 5061-5076, https://doi.org/10.5194/hess-18-5061-2014, 2014.

Yu, L., Zeng, Y., Su, Z., Cai, H., and Zheng, Z.: The effect of different evapotranspiration methods on portraying soil water dynamics and ET partitioning in a semi-arid environment in Northwest China, Hydrol Earth Syst Sci, 20, 975-990, https://doi.org/10.5194/hess-20-975-2016, 2016.

Yu, L., Zeng, Y., Wen, J., and Su, Z.: Liquid-Vapor-Air Flow in the Frozen Soil, Journal of Geophysical Research: Atmospheres, 123, 7393-7415, https://doi.org/10.1029/2018jd028502, 2018.

Yu, L., Fatichi, S., Zeng, Y., and Su, Z.: The role of vadose zone physics in the ecohydrological response of a Tibetan meadow to freeze–thaw cycles, The Cryosphere, 14, 4653-4673, https://doi.org/10.5194/tc-14-4653-2020, 2020a.

Yu, L., Zeng, Y., and Su, Z.: Understanding the mass, momentum, and energy transfer in the frozen soil with three levels of model complexities, Hydrol Earth Syst Sci, 24, 4813-4830, https://doi.org/10.5194/hess-24-4813-2020, 2020b.

Zeng, Y., Su, Z., Wan, L., and Wen, J.: Numerical analysis of air-water-heat flow in unsaturated soil: Is it necessary to consider airflow in land surface models?, Journal of Geophysical Research: Atmospheres, 116, D20107, https://doi.org/10.1029/2011JD015835, 2011a.

Zeng, Y., Su, Z., Wan, L., and Wen, J.: A simulation analysis of the advective effect on evaporation using a two-phase heat and mass flow model, Water Resour Res, 47, W10529, https://doi.org/10.1029/2011WR010701, 2011b.

Zeng, Y. J., and Su, Z. B.: STEMMUS : Simultaneous Transfer of Engery, Mass and Momentum in Unsaturated Soil, ISBN: 978-90-6164-351-7, University of Twente, Faculty of Geo-Information and Earth Observation (ITC), Enschede, 2013.

Zheng, D., Van der Velde, R., Su, Z., Wen, J., Booij, M. J., Hoekstra, A. Y., and Wang, X.: Under-canopy turbulence and root water uptake of a Tibetan meadow ecosystem modeled by Noah-MP, Water Resour Res, 51, 5735-5755, https://doi.org/10.1002/2015wr017115, 2015.